

4. Response Studies

4.1 Introduction

In this chapter, numerical experiments are presented which examine the generation and evolution of large-scale oceanic anomalies in response to anomalous wind forcing, on time scales of a month to a few years. Anomalous winds corresponding to a relaxation of the easterly winds in the equatorial region (section 4.2) and an intensification of the trade winds in the tropical and subtropical region (section 4.3) are imposed for several months. These wind anomalies are known as one of the atmospheric phenomena involved in ENSO (e. g., Rasmusson and Carpenter, 1982). Also is presented an additional experiment which demonstrates the evolution of an existing temperature anomaly under no anomalous wind forcing.

The experiments are summarized in Table 4-1-1. The corresponding anomalous winds and initial temperature anomaly are also shown in Fig. 4-1-1. Case 101 and case 201, whose normals are horizontally uniform and motionless, are the counterparts of case 100 and case 200.

Before anomaly experiments are carried out, the model is integrated over two years, starting from the state at the 140th year described in Chapter 3. During this integration and the following anomaly experiments, the heat and salinity fluxes through the ocean surface are kept to be the same as those at the end of the 140th year. This condition is chosen simply in order to isolate the effects of anomalous wind forcing and the ocean's internal adjustment mechanisms on anomaly development. The heat flux calculated according to Eq. (2-85) has a tendency to damp the temperature anomalies. The effects of anomalies in the surface heat and salinity fluxes on the generation and evolution of oceanic anomalies are not studied here.

The following description refers mainly to the temperature anomalies. *The anomaly of a variable is defined as the deviation from its normal which is obtained by the integration for the same period under no anomalous forcing.* Since the normal run is almost steady except in the deeper layers, the state is similar to that described in Chapter 3. The definition is employed because the temperature of the deeper layers changes slightly due to the vertical diffusion even in the absence of anomalous forcing. The prediction equation for a temperature anomaly can be written as

$$\frac{\partial T'}{\partial t} = -u' \frac{\partial \bar{T}}{\partial \lambda} - v' \frac{\partial \bar{T}}{\partial \phi} - \bar{u} \frac{\partial T'}{\partial \lambda} - \bar{v} \frac{\partial T'}{\partial \phi} - w' \frac{\partial \bar{T}}{\partial z} - \bar{w} \frac{\partial T'}{\partial z} - u' \frac{\partial T'}{\partial \lambda} \quad \text{(A) (B) (C) (D) (E) (F) (G)}$$

Table 4-1-1 Description of the experiments, (a) response to anomalous wind forcing and (b) evolution of an initial temperature anomaly. τ^λ indicates the normal wind stress. Period means the term for which anomalous winds are imposed. The normal state (*) is almost identical to the quasi-steady state described in Chapter 3, while that (**) for case 101 and case 201 is horizontally uniform and motionless.

(a)

case	anomalous wind stress	period (days)	normal state
100	$0.35 \cdot \sin\left(\frac{\lambda-1.25}{65}\pi\right) \cdot \frac{1}{2}\{1+\cos\left(\frac{\phi}{10}\pi\right)\}$	90	*
101	$1.25 \leq \lambda \leq 66.25$ $-9 \leq \phi \leq 9$	90	**
110	$ \tau^\lambda(\phi) $ $1.25 \leq \lambda \leq 28.75$ $-9 \leq \phi \leq 9$	90	*
120	$ \tau^\lambda(\phi) $ $36.25 \leq \lambda \leq 63.75$ $-9 \leq \phi \leq 9$	90	*
130	$ \tau^\lambda(\phi) $ $71.25 \leq \lambda \leq 98.75$ $-9 \leq \phi \leq 9$	90	*
200	$-0.35 \cdot \sin\left(\frac{\lambda-33.75}{65}\pi\right) \cdot \frac{1}{2}\{1+\cos\left(\frac{\phi-15}{15}\pi\right)\}$	180	*
201	$33.75 \leq \lambda \leq 98.75$ $1 \leq \phi \leq 29$	180	**
210	$- \tau^\lambda(\phi) $ $51.25 \leq \lambda \leq 98.75$ $11 \leq \phi \leq 29$	90	*

(b)

case	initial temperature anomaly	normal state
250	$3 \cdot \cos\left(\frac{\lambda-50}{25}\pi\right) \cdot \cos\left(\frac{\phi-14}{12}\pi\right)$ $37.5 \leq \lambda \leq 62.5$ $8 \leq \phi \leq 20$ $-380 \leq z \leq 0$	*

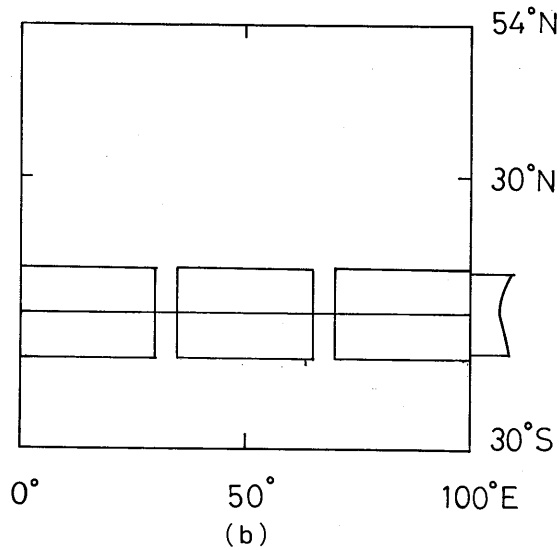
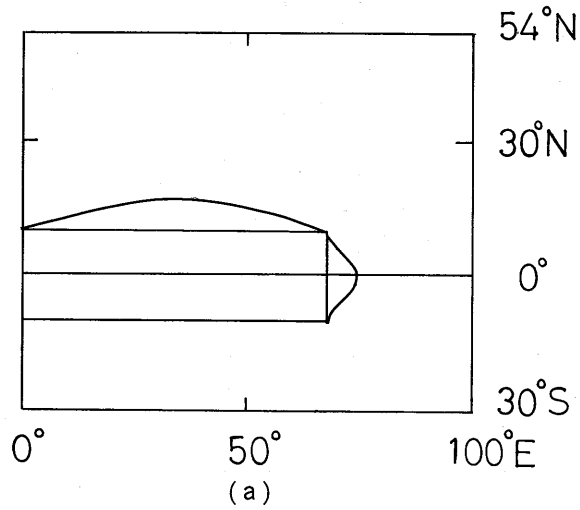


Fig. 4-1-1 Location and structure of the anomalous zonal wind stress, (a) case 100 and case 101, (b) case 110, case 120, and case 130, (c) case 200 and case 201, (d) case 210 and (e) location and structure of the initial temperature anomaly of case 250. The zonal and meridional structures, unless they are zonally uniform, are shown along the longitude and latitude through the centers of the anomalously forced regions. The initial anomaly of case 250 uniformly extends from the surface to 380 m depth.

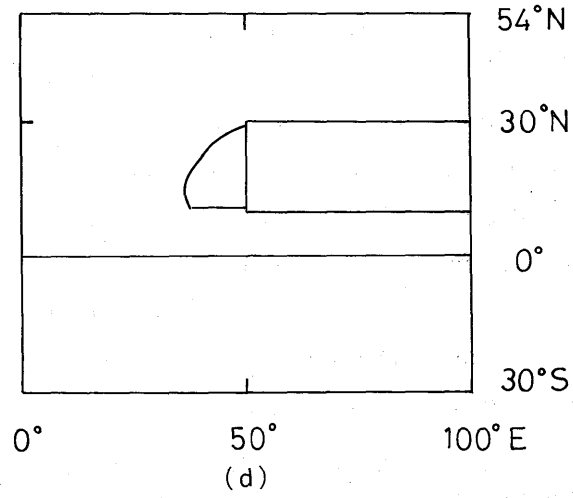
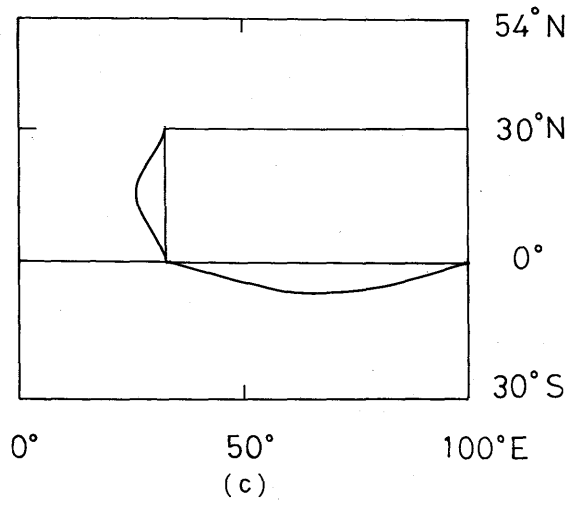


Fig. 4-1-1 Continued.

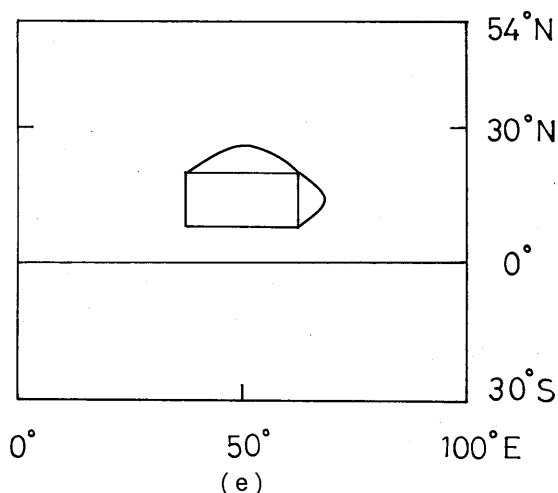


Fig. 4-1-1 Continued.

$$\begin{aligned}
 & -v' \frac{\partial T'}{a \partial \phi} - w' \frac{\partial T'}{\partial z} + A_h \nabla^2 T' + \frac{K_h}{\delta} \frac{\partial^2 T'}{\partial z^2}, \quad (4-1) \\
 & \quad \quad \quad \text{(H)} \quad \quad \text{(I)} \quad \quad \text{(J)} \quad \quad \text{(K)}
 \end{aligned}$$

where the overbars denote the normals, and primes the anomalies. Terms (A), (B), and (E) denote the effect of advection of normal temperature field by anomalous currents, terms (C), (D), and (F) the effect of advection of anomalous temperature field by normal currents, and terms (G), (H), and (I) the effect of advection of anomalous temperature field by anomalous currents. Terms (J) and (K) are the diffusive change of anomalous temperature. If the normal state is horizontally uniform and motionless, as in case 101 and case 201, terms (A), (B), (C), (D), and (F) are always zero, and term (E) plays the most important role in the initial development of temperature anomalies.

It would be helpful for describing the oceanic response to tabulate the characteristics of the vertical normal modes in the model ocean in advance. Typical values for the first three baroclinic modes are given in Table 4-1-2 for a few typical stratifications. h is the equivalent depth associated with the given mode. $c = \sqrt{gh}$ is the phase speed of the corresponding gravity wave. L_R , the Rossby radius of deformation, is a characteristic horizontal length scale. c_R is the westward phase speed of the non-dispersive Rossby wave :

$$c_R = \frac{1}{3} \sqrt{gh} = \frac{1}{3} c \quad (\text{for an equatorial mode with meridional mode number } 1),$$

Table 4-1-2 Characteristics of the first three baroclinic modes in the model ocean, (a) (0°, 50°E), (b) (6°N, 50°E), and (c) (18°N, 50°E). d and y in the last line indicate that the unit is day and year, respectively.

	(a)			(b)			(c)		
mode	1	2	3	1	2	3	1	2	3
h cm	133	40	18	132	42	18	140	37	17
c cm/s	361	198	132	360	203	134	371	191	128
L_R km	397	294	240	236	133	88	82	42	28
c_R cm/s	120	66	44	127	40	17	15	3.9	1.8
T_R	107d	195d	294d	101d	318d	2.0y	2.3y	8.6y	19.1y

$$= \frac{\beta g h}{f^2} \quad (\text{for an off-equatorial mode}). \quad (4-2)$$

where β is the northward gradient of the Coriolis parameter f ($=2\Omega \sin\phi$). The eastward phase speed of the equatorially trapped Kelvin wave is equal to c . T_R indicates the time required for the Rossby wave to propagate from the eastern to the western boundary at each latitude. Fig. 4-1-2 shows the eigen modes of temperature change associated with the first three baroclinic modes. These changes arise through term (E) in Eq. (4-1). If we project the wind stress which acts as a body force in the uppermost layer into the vertical normal modes for the equatorial region, the second baroclinic mode is shown to have a slightly larger projection than the first. (Figures appearing in sections 4.2 and 4.3 are summarized in Table 4-1-3.)

4.2 Response to anomalous forcing in the equatorial ocean

4.2.1 Anomalous eastward wind (cases 100 and 101)

In case 100, anomalous eastward winds are imposed in the western two-thirds of the equatorial region (10°S—10°N) for 90 days (day 1—day 90) (Table 4-1-1(a), Fig. 4-1-1(a)). The maximum wind stress anomaly of 0.35 dyne/cm² nearly cancels the normal westward wind stress on the equator. There are no oceanic anomalies at the initial time. This experiment is intended to examine the oceanic response to *an abrupt relaxation of the easterly winds in the western equatorial ocean.*

Case 101 is an experiment which employs the same anomalous winds as case 100, whereas the initial state is horizontally uniform and motionless. The initial temperature and salinity

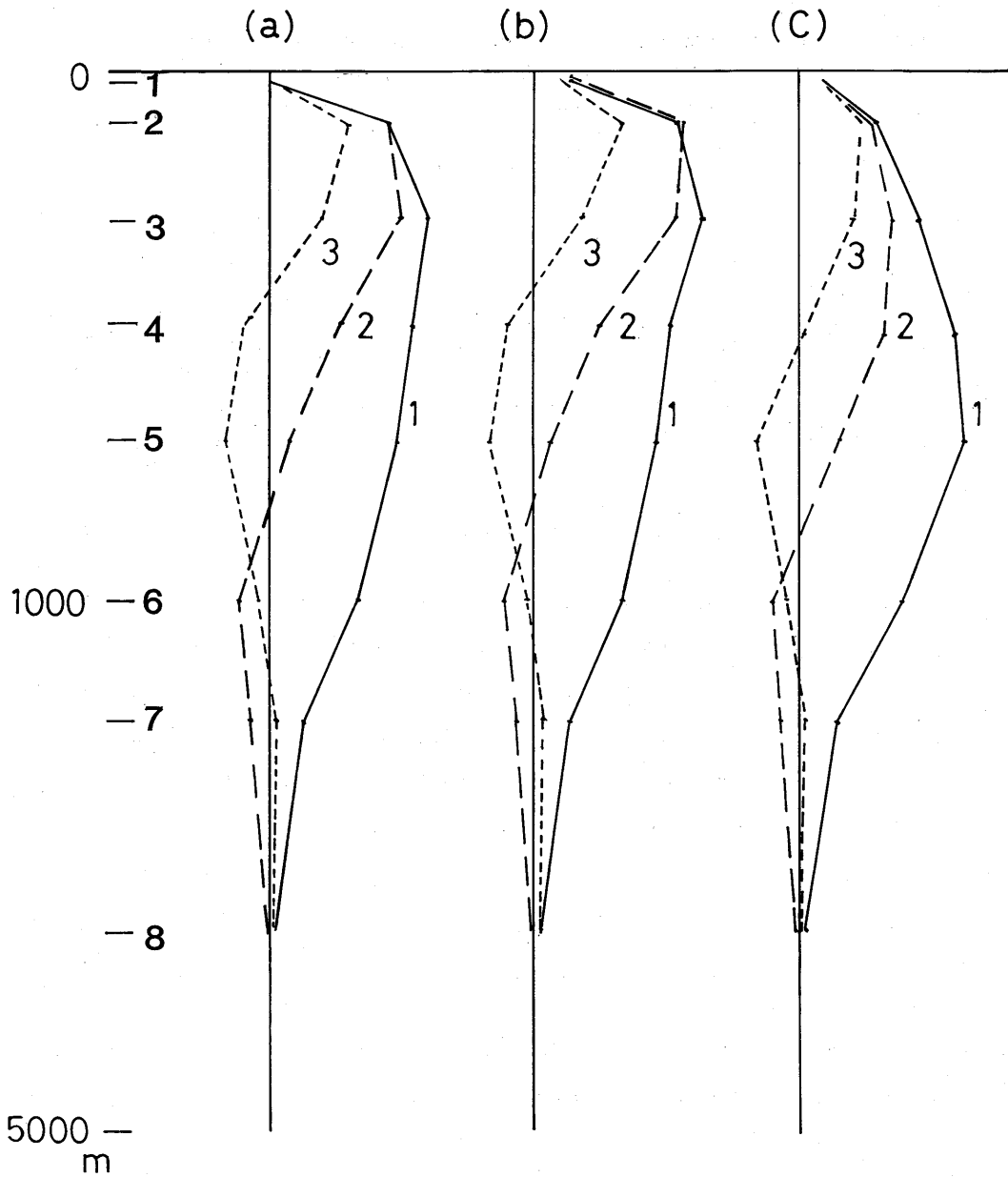


Fig. 4-1-2 Vertical structure of the temperature changes associated with the first three baroclinic modes, (a) (0°, 50°E), (b) (6°N, 50°E), and (c) (18°N, 50°E). Horizontal scale is arbitrary.

are those obtained by averaging the initial state of case 100 over the region from 10°S to 10°N and from 0° to 100°E. In this section, the results of case 100 are described first, then they are compared with those of case 101.

Table 4-1-3 List of figure numbers given in sections 4.2 and 4.3. λ , ϕ , z , k and t are longitude, latitude, height, level, and time, respectively. Units of (λ, ϕ) and t are degree and day, respectively.

Anomaly Case	$T'(\lambda, \phi)$ $t=90$	$T'(\lambda, \phi)$ $t=120$	$T'(\lambda, \phi)$ $t=180$	$T'(\lambda, \phi)$ $t=300$	$T'(\lambda, \phi)$ $t=360$	$T'(\lambda, \phi)$ $t=720$	$T'(\phi, z)$ $t=90$	$T'(\phi, z)$ $t=180$	$T'(\lambda, z)$ $\phi=0$	$T'(\lambda, z)$ $\phi=6$	$T'(\lambda, z)$ $\phi=14$	$T'(\lambda, z)$ $\phi=18$	$T'(\lambda, t)$ $\phi=0$	$T'(\lambda, t)$ $\phi=6$	$T'(\lambda, t)$ $\phi=18$	$T'(\phi, t)$ $k=1$	$u'(\lambda, t)$ $\phi=0$	Others
100	4-2-2 (a)k=1 (b)k=2		4-2-6 (a)k=1 (b)k=2		4-2-7 (a)k=1 (b)k=2		4-2-3 (a) $\lambda=15$ (b) $\lambda=85$	4-2-4 (a) $\lambda=15$ (b) $\lambda=85$	4-2-5 (a)t=90 (b)t=180				4-2-8 (a)k=1 (b)k=2			4-2-10 (a) $\lambda=0$ (b) $\lambda=10$	4-2-9 (a)k=1 (b)k=2	4-2-1
101	4-2-11 (a)k=1 (b)k=2												4-2-12 (a)k=1 (b)k=2					
110	4-2-13 (a)k=1 (b)k=2		4-2-13 (c)k=1 (d)k=2										4-2-14 (a)k=1 (b)k=2				4-2-14 (c)k=1 (d)k=2 (e)k=6	
120													4-2-15 (a)k=2				4-2-15 (b)k=1	
130	4-2-17 (a)k=1 (b)k=2		4-2-17 (c)k=1 (d)k=2										4-2-16 (a)k=2				4-2-16 (b)k=1	
200			4-3-1 (a)k=1 (b)k=3		4-3-4 (a)k=1 (b)k=3	4-3-5 (a)k=1 (b)k=3			4-3-3 (b)t=180		4-3-3 (a)t=180		4-3-7 (a)k=1 (b)k=3	4-3-6 (a)k=1 (b)k=3				4-3-2 4-3-8
201					4-3-9 (a)k=1 (b)k=3													
250		4-3-10 (a)k=1 (b)k=4		4-3-12 (a)k=1 (b)k=4								4-3-11 t=120						

The relaxation of the easterly winds results in an eastward acceleration in the upper ocean because of the initial eastward pressure force balanced with the normal westward wind stress.

Therefore, the westward equatorial current of the uppermost level decelerates, and then reverses its direction. This is evident in Fig. 4-2-1, which shows the evolution of the surface currents along the equator (see also Fig. 4-2-9(a)). As a result, the westward advection of the cold water upwelled on the equator weakens, and then an eastward advection of the warm water pooled in the western equatorial region takes place.

In the meridional section, anomalous equatorward convergent currents are induced in the surface layer, which are compensated by downwelling on the equator, upwelling on both sides of it, and poleward divergent motion at depth. This anomalous meridional circulation tends to raise the surface temperature along the equator by means of suppression of the equatorial upwelling, and also by horizontal heat advection since the normal temperature is maximum at 8°N and 8°S (Fig. 3-3(a)). Due to the combined effects of the anomalous horizontal and vertical advectons of normal temperature field (terms (A), (B), and (E) in Eq. (4-1)), anomalous temperatures initially develop in the forced region. Moreover, unforced regions may be affected by Kelvin and Rossby waves or advection of anomalies by normal currents.

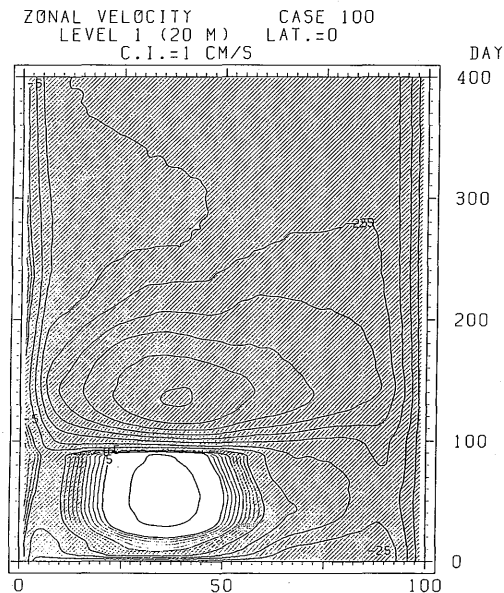


Fig. 4-2-1 Zonal velocity variations along the equator at level 1 in case 100. Shaded areas indicate westward flow.

Fig. 4-2-2 shows the temperature anomalies of level 1 and level 2 on day 90 when the anomalous winds are instantaneously turned off. A warm anomaly is formed along the equator at level 1. The anomaly is extended poleward along the eastern boundary. On either side of the equator, cold anomalies are formed along 8°N and 8°S . The anomaly pattern of level 2 is widely different from that of level 1. Anomalously cold water is developed under the surface warm anomaly in the western part of the forced region.

In the unforced equatorial region and along the eastern boundary warm anomalies develop at both levels. Magnitudes of the anomaly near the eastern boundary are larger at level 2 than at level 1. The cold anomalies of both level 1 and level 2 are centered at the latitudes where the normal temperature is maximum, i. e., 8°N and 8°S at level 1 and 4°N and 4°S at level 2. The pattern of level 2 is fairly similar to that of Fig. 6.6 in Leetmaa et al. (1981), which shows the adjustment of the model thermocline topography after a weakening of the westward trade winds in a longitudinally and latitudinally confined region.

Meridional sections within and east of the forced region are shown in Figs. 4-2-3 and 4-2-4. There is considerable difference in the development of anomalies between the forced and the unforced region. The anomaly pattern at 15°E on day 45 (not shown) is similar to that on day 90. At 85°E , on the other hand, the pattern changes between day 45 and day 90, which reflects the appearance of a deep cold anomaly after day 45.

The longitudinal dependence of the vertical structure is also evident in Fig. 4-2-5(a). The warm anomaly seen in Fig. 4-2-2(a) is confined to the uppermost level in the western half of the forced region, while it extends down to level 3 in the eastern half. Near the eastern boundary the warm anomaly penetrates to a deeper level and has a maximum value at level 2.

When the anomalous winds are turned off, the normal westward wind stress causes westward acceleration in the upper ocean since the normal eastward pressure force has already collapsed during the first 90 days. A much faster jet than the normal westward equatorial current appears for a certain period due to the acceleration (see Figs. 4-2-1 and 4-2-9(a)).

The temperature anomalies on day 180 are shown in Fig. 4-2-6. The cold and warm anomalies of level 1 that existed in the equatorial region on day 90 have moved away from the equator. Along the equator, cold anomalies are newly formed both at level 1 and level 2. Changes in meridional sections are seen in Figs. 4-2-3 and 4-2-4. (The warm anomalies centered at 20°N and 20°S in Fig. 4-2-4(b) are due to the convective adjustment.) The

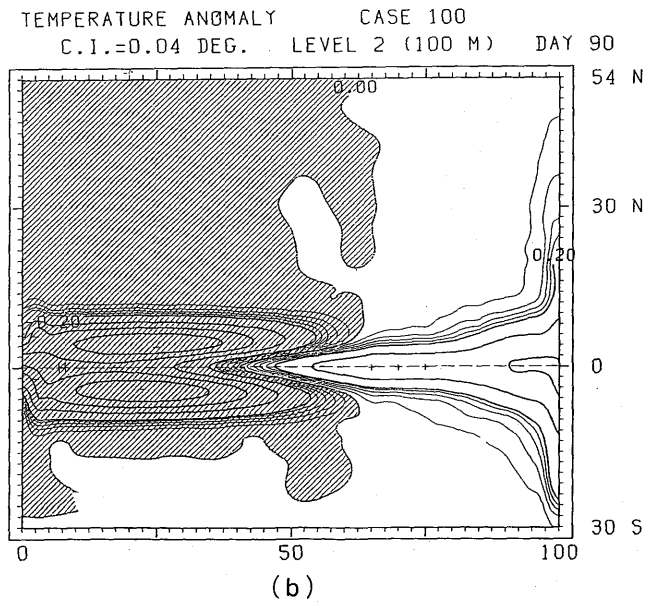
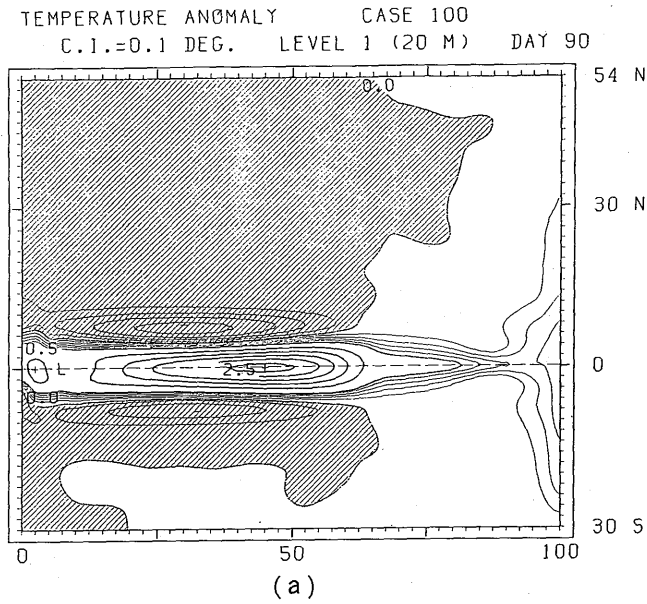
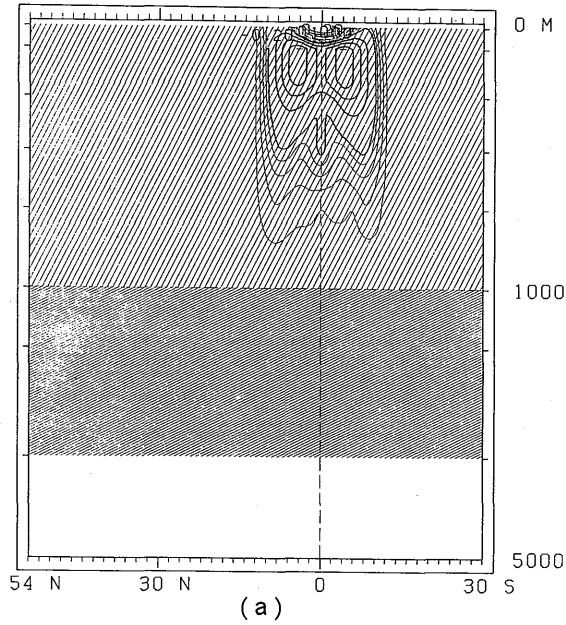


Fig. 4-2-2 Temperature anomalies on day 90 in case 100. (a) Level 1 and (b) level 2. Negative anomalies are shaded. *C.I.* indicates the interval of thin lines, while the interval of bold lines is five times *C.I.*. + and *L* indicate maximum and minimum in positive anomalies, and - and *H* indicate maximum and minimum in negative anomalies, respectively.

TEMPERATURE ANOMALY CASE 100
C.I.=0.04 DEG. LONG. =15.0 DAY 90



TEMPERATURE ANOMALY CASE 100
C.I.=0.04 DEG. LONG. =85.0 DAY 90

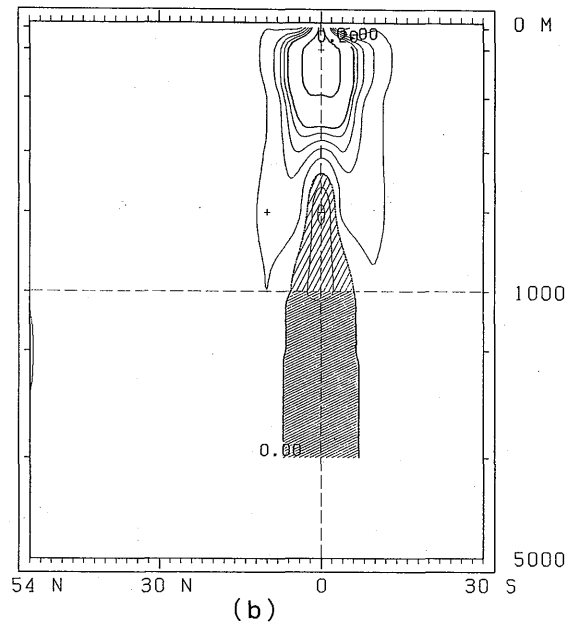
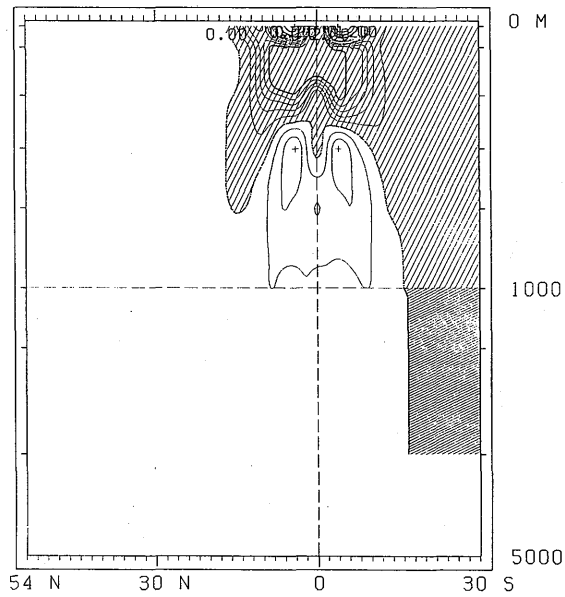


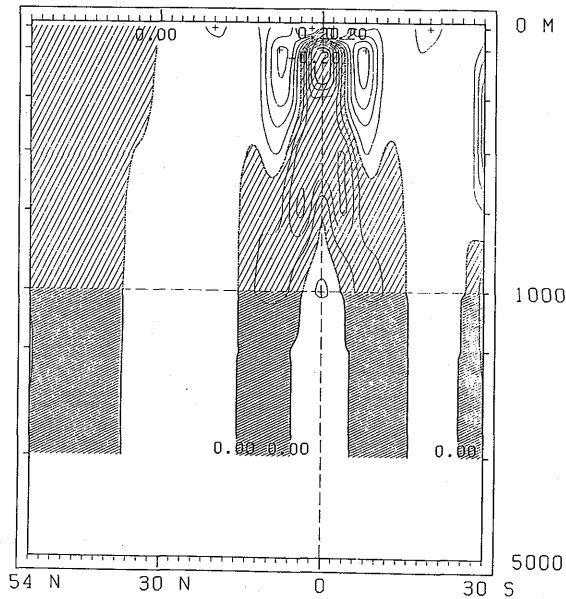
Fig. 4-2-3 Meridional cross-sections of the temperature anomalies on day 90 in case 100. (a) Along 15°E and (b) along 85°E.

TEMPERATURE ANOMALY CASE 100
C.I.=0.04 DEG. LONG. =15.0 DAY 180



(a)

TEMPERATURE ANOMALY CASE 100
C.I.=0.04 DEG. LONG. =85.0 DAY 180



(b)

Fig. 4-2-4 As in Fig. 4-2-3 except for day 180.

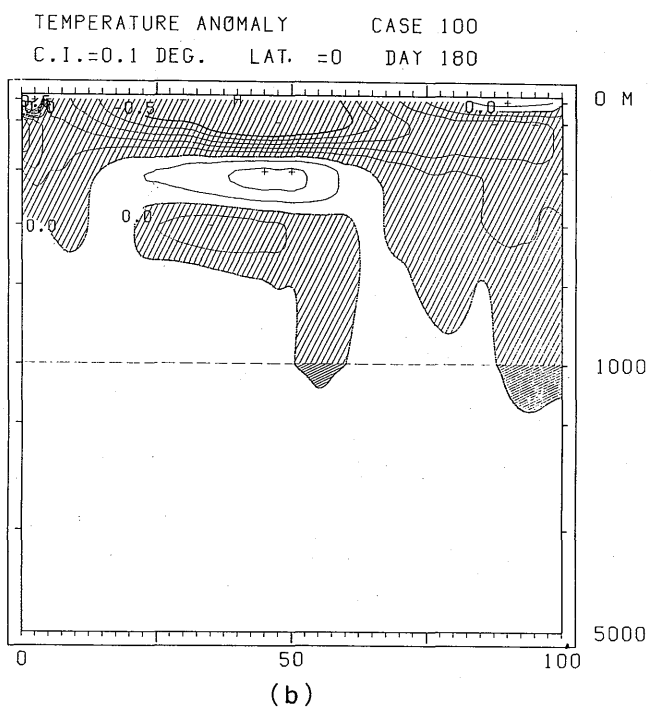
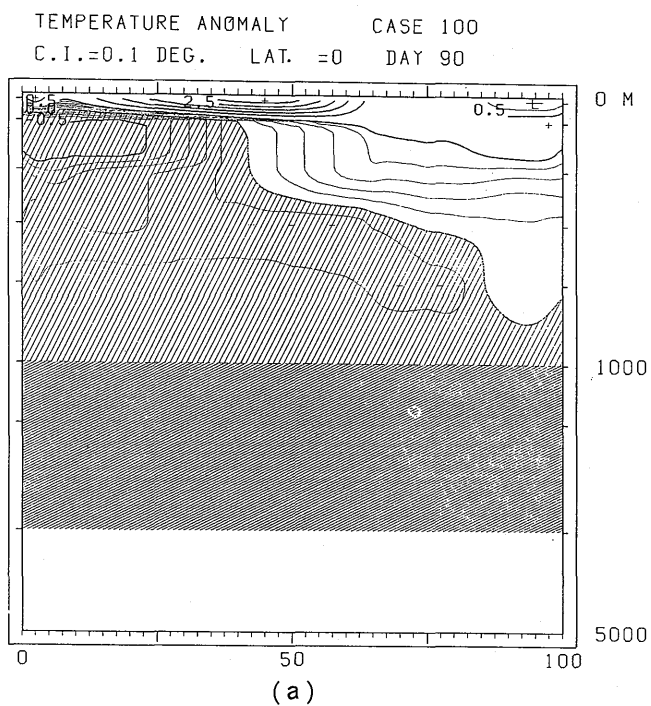


Fig. 4-2-5 Zonal cross-sections of the temperature anomalies along the equator in case 100. (a) Day 90 and (b) day 180.

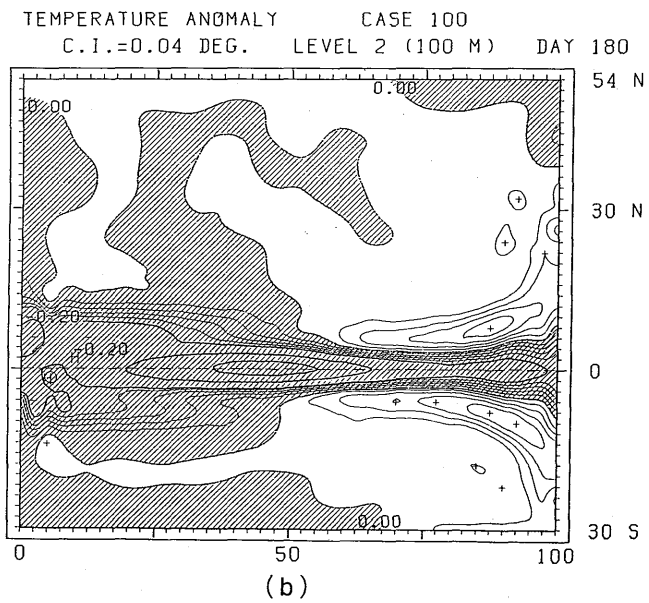
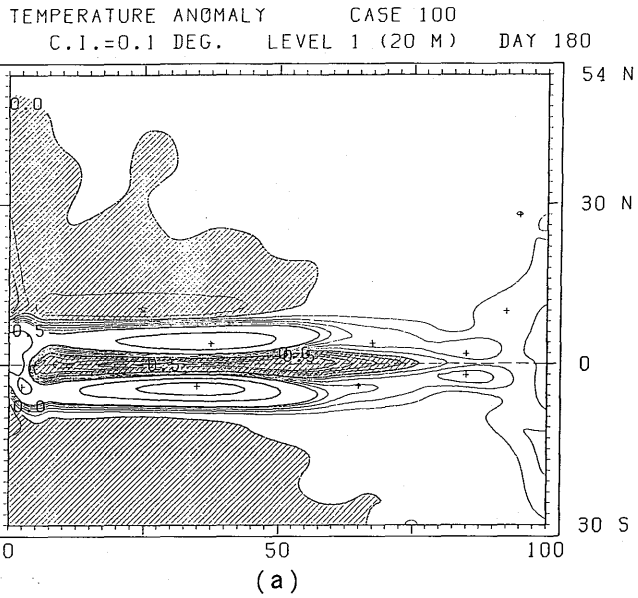


Fig. 4-2-6 As in Fig. 4-2-2 except for day 180.

section along the equator shown in Fig. 4-2-5(b) is entirely different from that on day 90.

It is not easy to identify which terms in Eq. (4-1) are responsible for the development of anomalies after day 90, since the anomalies produced during the first 90 days are large enough to change the normal state significantly. However, advection of anomalies by normal currents can presumably explain the anomaly development along the equator to some extent. At level 1, after anomalous forcing was switched off, the upwelling of cold water and poleward advection of warm water tend to diminish the existing warm anomaly, and then to generate a cold anomaly. At level 2, the normal equatorial motion converges the cold water on the equator and advects to the east.

Fig. 4-2-7 shows the temperature anomalies on day 360. The newly produced cold anomaly of level 1 is also split into two centers. At level 2, the cold anomaly along the equator is almost stationary.

Fig. 4-2-8 shows the temperature anomaly variations along the equator at level 1 and level 2. At level 1, anomalous water, both warm and cold, develops in the anomalously forced region. At level 2, the relatively fast eastward movement of a warm anomaly center and slow movement of a cold anomaly center are seen.

Fig. 4-2-9 shows the variations of the zonal velocity anomalies. At level 1, velocity anomalies are produced in the anomalously forced region. However, the phase of the velocity anomalies does not coincide with that of the temperature anomalies. The zonal velocity anomaly u' basically develops as a result of imbalance between pressure force and wind stress. The anomaly u' produced strongly affects the temperature anomaly development through the term $u' \partial \bar{T} / \partial x$ in Eq. (4-1). As long as u' does not change sign, the contribution of $u' \partial \bar{T} / \partial x$ to the anomaly development $\partial T' / \partial t$ has the same sign. It results in a delay of the phase of the temperature anomalies. At level 2, both eastward and westward displacements of anomalies are seen. When the easterly winds relax, the eastward current anomalies develop and the eastward equatorial undercurrent accelerates. Then the undercurrent decelerates (except near the western edge) due to weakening of the eastward pressure force in the upper ocean, and subsequently dies out in the eastern forced region. For a short period after day 90, westward currents appear. Then the equatorial undercurrent reappears.

As seen in Figs. 4-2-6 and 4-2-7, anomalies drift or extend poleward along the western boundary. The northward movement of the anomalies formed to the north of the equator is obvious from Fig. 4-2-10, which shows the surface temperature anomaly variations near the

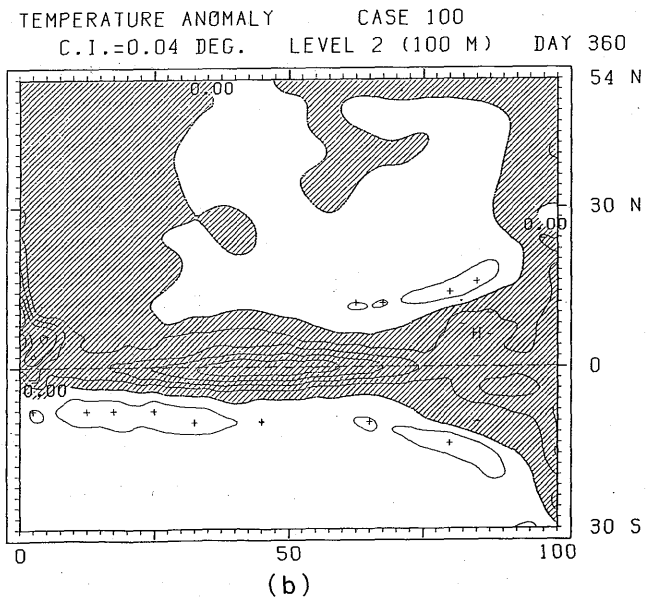
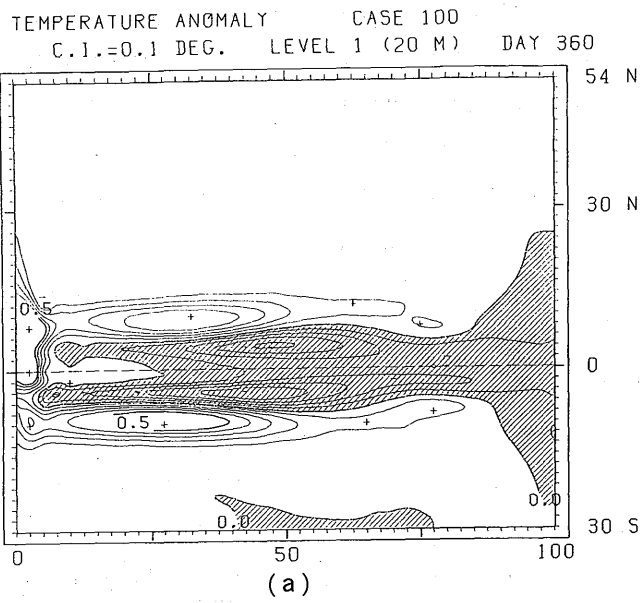


Fig. 4-2-7 As in Fig. 4-2-2 except for day 360.

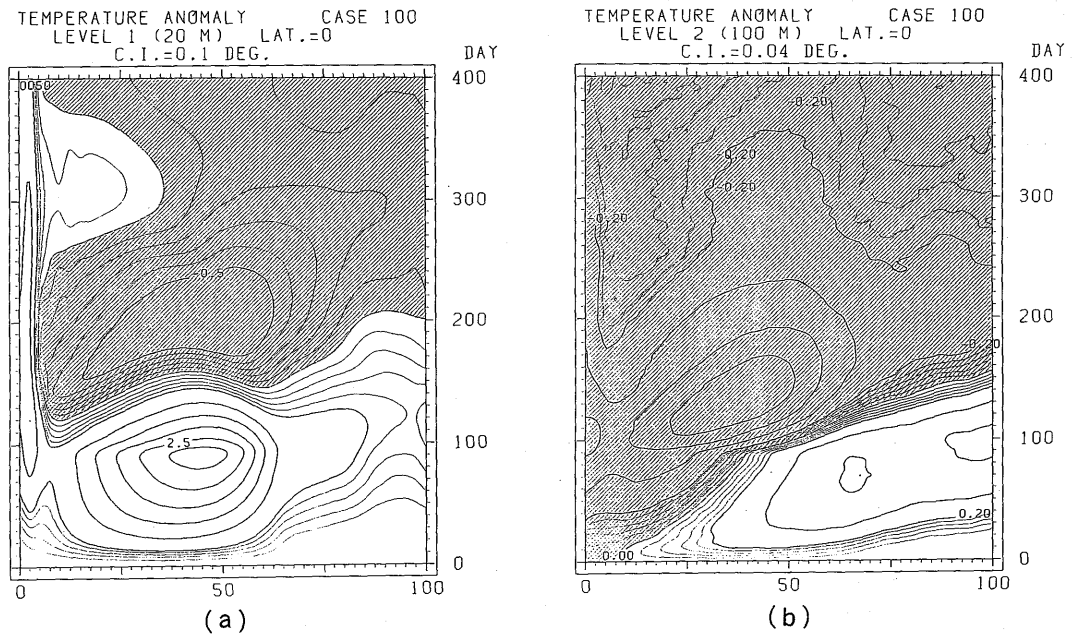


Fig. 4-2-8 Temperature anomaly variations along the equator in case 100.
(a) Level 1 and (b) level 2.

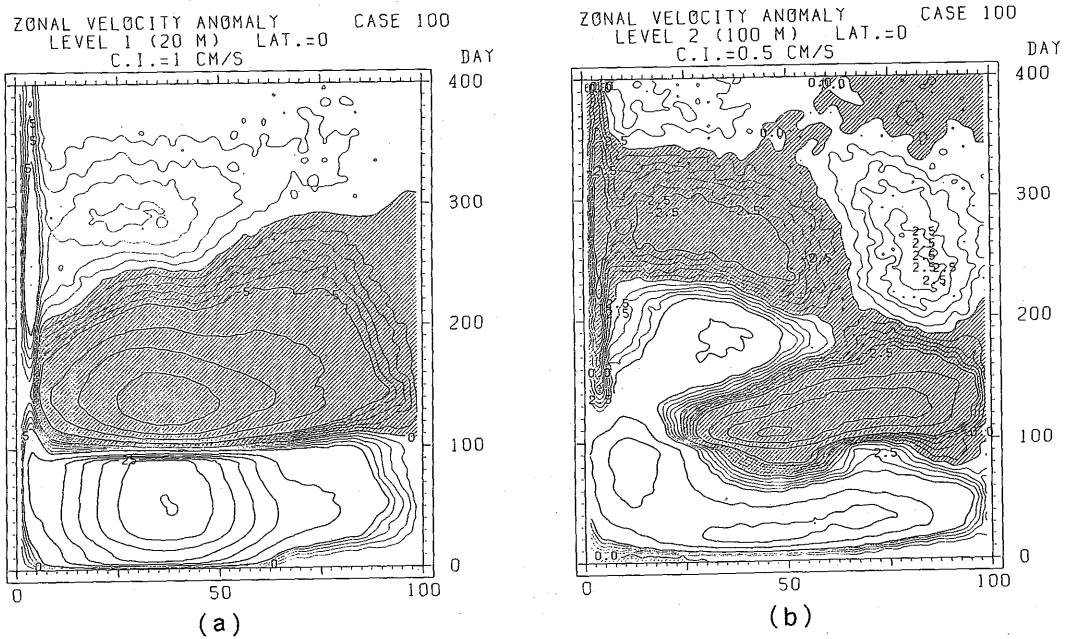
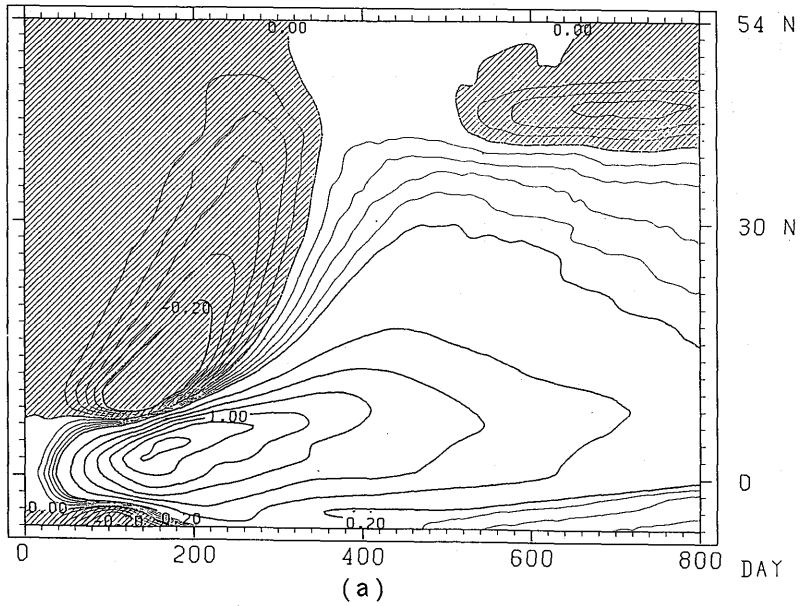


Fig. 4-2-9 As in Fig. 4-2-8 except for the zonal velocity anomalies.

TEMPERATURE ANOMALY CASE 100
LEVEL 1 (20 M) LONG.=0.0
C.I.=0.04 DEG.



TEMPERATURE ANOMALY CASE 100
LEVEL 1 (20 M) LONG.=10.0
C.I.=0.02 DEG.

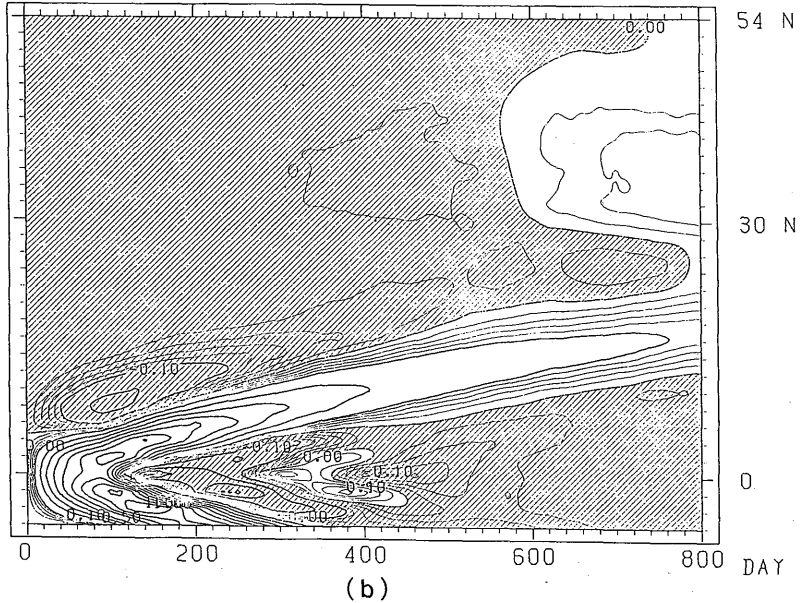


Fig. 4-2-10 Temperature anomaly variations at level 1 in case 100.
(a) Along the western boundary and (b) 10°E.

western boundary. The movement, 25° in latitude in 100 days at the western boundary (Fig. 4-2-10(a)) and 20° in 600 days at 10°E (Fig. 4-2-10(b)), is equivalent to speeds of about 30 cm/sec and 4 cm/sec, respectively. They are nearly equal to the normal current speed at the uppermost level (cf. Fig. 3-3 (d)). The cold anomaly which is seen at the western boundary north of 40°N after day 500 is partially due to surfacing of the cold water advected northward at level 2. The anomalous water north of 30°N at 10°E is advected eastward from the western boundary region.

Now, compare case 101 with case 100 in order to clarify the role of the normal temperature and currents on the anomaly development.

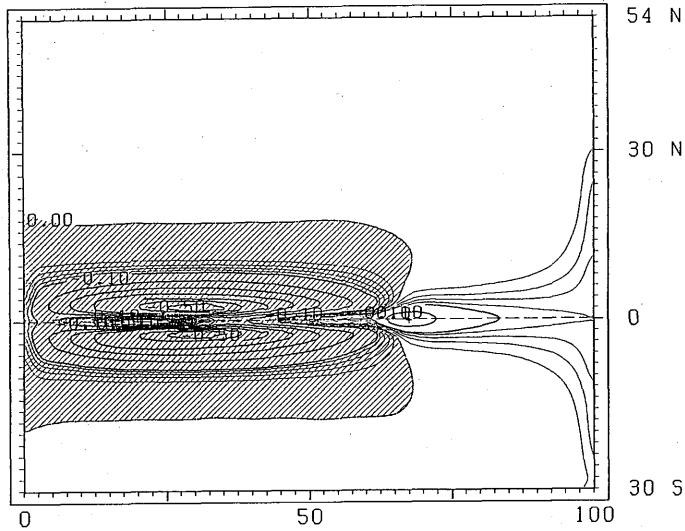
The results of case 101, the horizontal temperature anomaly distribution on day 90 and the temperature anomaly variations along the equator, are shown in Figs. 4-2-11 and 4-2-12. The largest difference between Figs. 4-2-2 and 4-2-11 is in the intensity and extent of surface warm anomaly in the anomalously forced region. In case 101, the warm water is only slightly seen on the equator. This difference in the anomaly development on the equator is also evident from Figs. 4-2-8(a) and 4-2-12(a).

In case 100, the surface warm anomaly in the forced region continues to grow until anomalous winds are turned off. In case 101, on the other hand, it ceases to grow halfway, and then begins to diminish except near the eastern edge. Vertical currents induced by the anomalous winds generate a warm anomaly on the equator in both cases. In case 101, however, once cold anomalies are generated by upwelling on both sides of the equator, the equatorward advection by meridional circulation comes into play. In case 100, as explained above, the eastward advection of normal temperature field by longitudinal circulation plays an important role in generating the warm anomaly. This process, further, is able to explain a relatively large magnitude of the warm anomaly near the eastern boundary in case 100 compared to case 101.

The anomaly distribution at level 2 is not so different as that at level 1. However, two differences between Figs. 4-2-8(b) and 4-2-12(b) are noted. One is that the warm anomaly in the forced region grows more rapidly in case 101 than in case 100. The other is that the eastward expansion of the cold anomaly region is swifter in case 100.

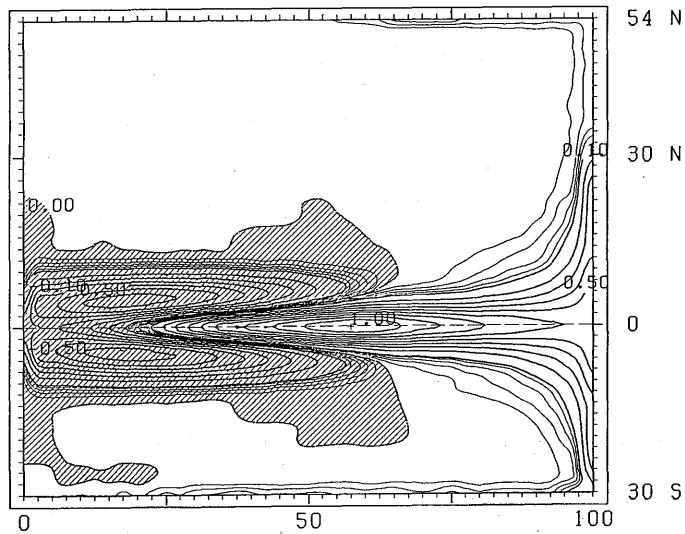
The evolutions after day 90 are very different between the two cases. All anomalies simply diminish to zero in case 101.

TEMPERATURE ANOMALY CASE 101
C.I.=0.02 DEG. LEVEL 1 (20 M) DAY 90



(a)

TEMPERATURE ANOMALY CASE 101
C.I.=0.02 DEG. LEVEL 2 (100 M) DAY 90



(b)

Fig. 4-2-11 As in Fig. 4-2-2 except for case 101.

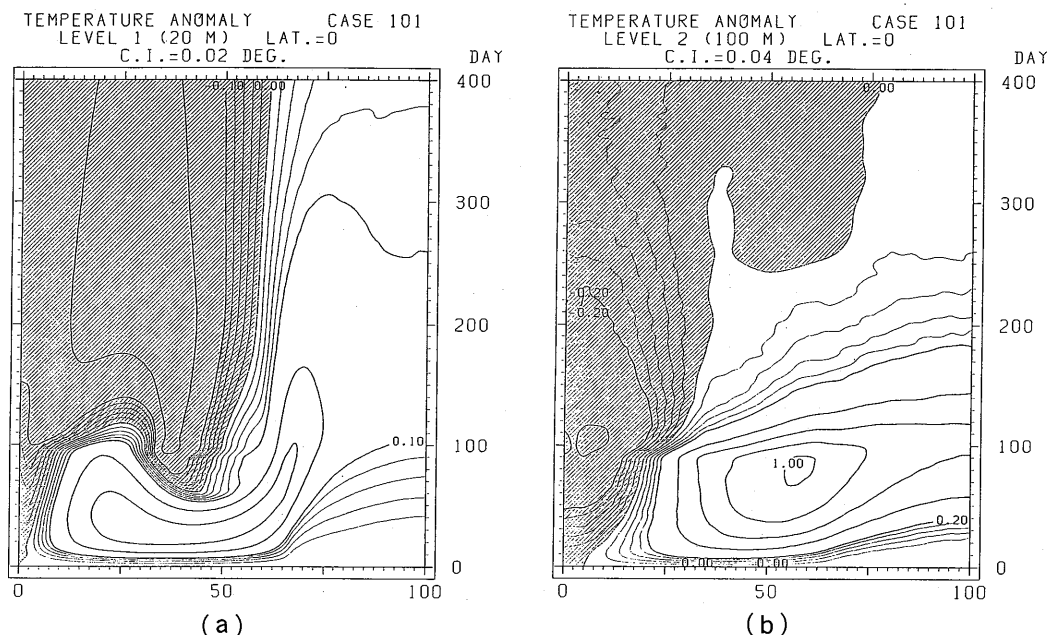


Fig. 4-2-12 As in Fig. 4-2-8 except for case 101.

4.2.2 Effect of the difference in the longitude of the forcing anomaly (cases 110, 120 and 130)

In this section, three experiments are described, in which anomalous eastward winds are imposed in the western, central, and eastern thirds of the equatorial region (10°S–10°N), respectively (Table 4-1-1(a), Fig. 4-1-1(b)). The purpose of the experiments is to see how the generation and evolution of anomalies depend on the longitudinal location of the anomalously forced region. The anomalous winds are introduced by stopping the normal westward winds in each region for 90 days.

Figs. 4-2-13 and 4-2-14 show the results of case 110. They are qualitatively similar to the results of case 100, but there are some differences caused by the change in the anomalous wind forcing region (cf. Figs. 4-2-2, 4-2-6, 4-2-8, and 4-2-9).

Firstly, the cold anomalies on both sides of the equator on day 90 are centered at latitudes further poleward. Secondly, the warm anomalies in the unforced region are smaller. Thirdly, Kelvin and Rossby waves are more clearly discernible. The reason for the last difference is that the western and eastern edges of the anomalous winds are more sharply defined in case 110. When the anomalous winds are imposed or turned off, Kelvin and Rossby waves are excited at each of the edges. In addition to these waves, Rossby waves are excited at the eastern boundary due to the reflection of the initially excited Kelvin

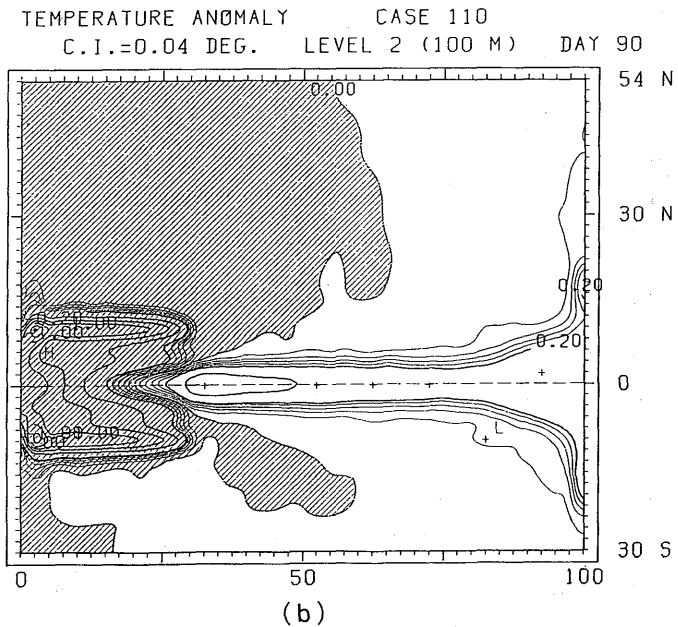
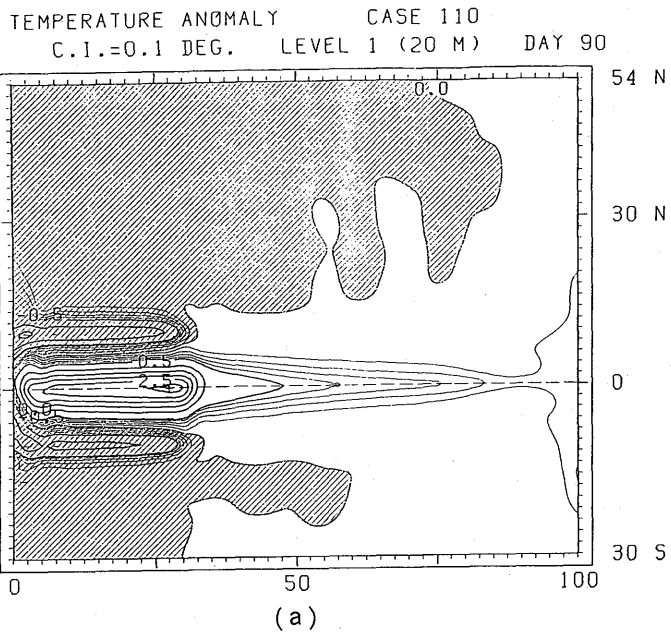
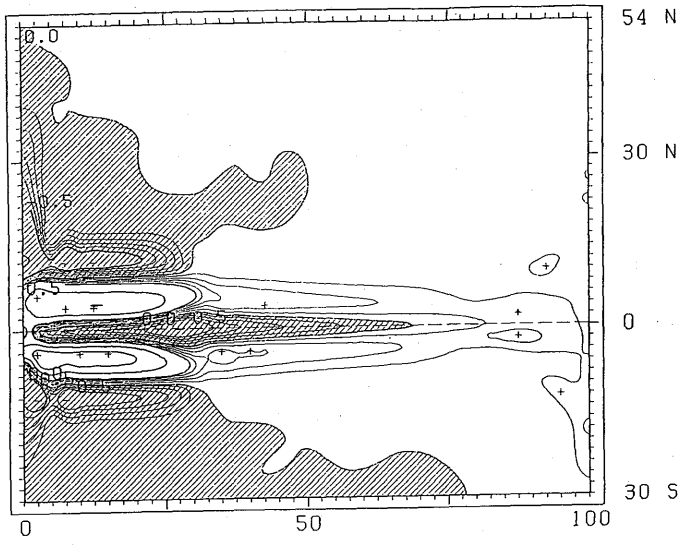


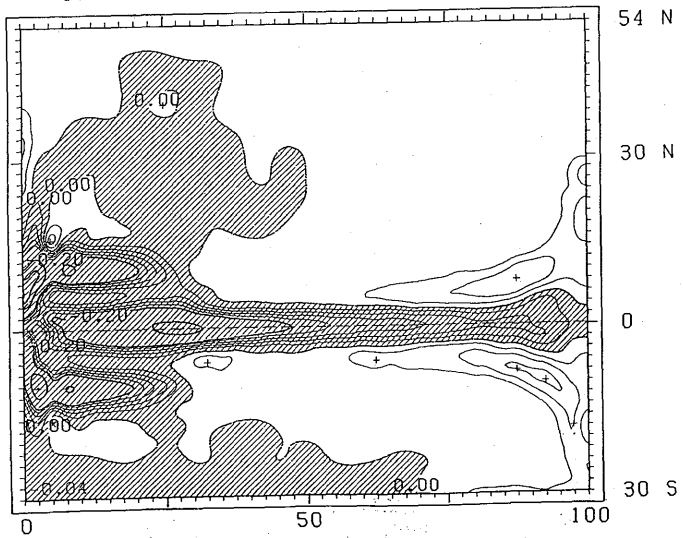
Fig. 4-2-13 Temperature anomalies in case 110. (a) Level 1 and (b) level 2 on day 90, and (c) level 1 and (d) level 2 on day 180.

TEMPERATURE ANOMALY CASE 110
C.I.=0.1 DEG. LEVEL 1 (20 M) DAY 180



(c)

TEMPERATURE ANOMALY CASE 110
C.I.=0.04 DEG. LEVEL 2 (100 M) DAY 180



(d)

Fig. 4-2-13 Continued.

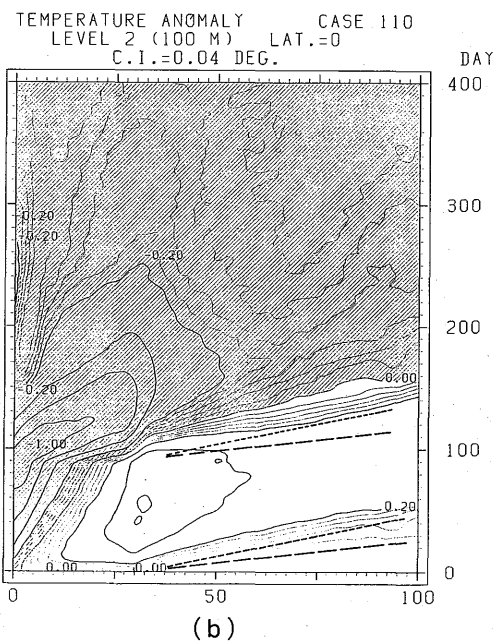
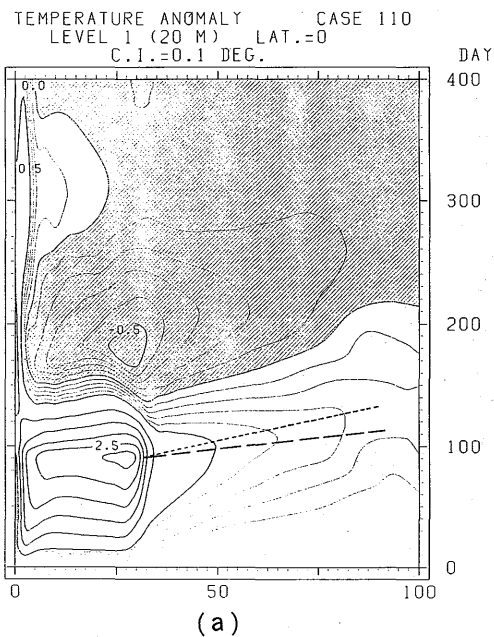


Fig. 4-2-14 Evolution of the conditions along the equator in case 110. The temperature anomalies at (a) level 1 and (b) level 2, and the zonal velocity anomalies at (c) level 1, (d) level 2, and (e) level 6. The dashed lines and the dotted lines correspond to Kelvin and non-dispersive Rossby waves of the first baroclinic mode and the second baroclinic mode, respectively.

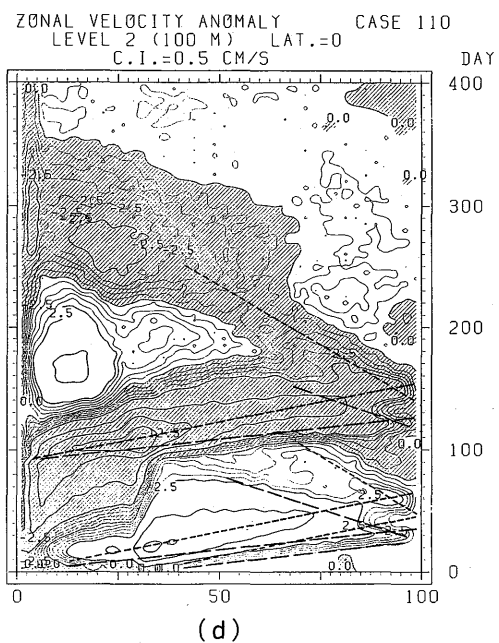
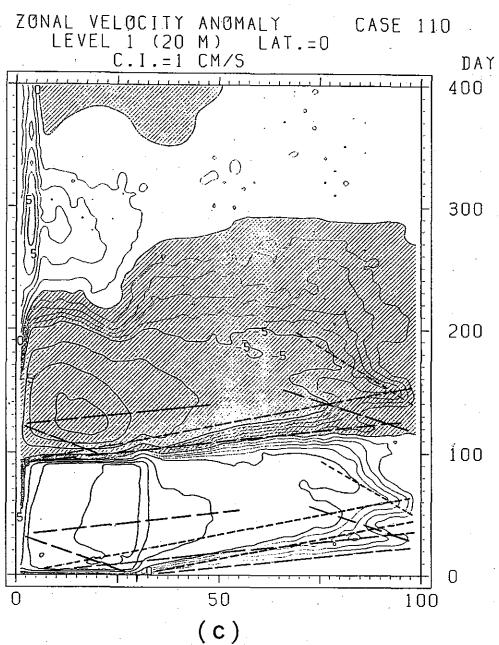


Fig. 4-2-14 Continued.

waves, and Kelvin waves are excited at the western boundary due to the reflection of the initially excited Rossby waves. The dashed lines and dotted lines in Fig. 4-2-14 correspond to the first baroclinic mode and second baroclinic mode Kelvin and non-dispersive Rossby waves. The horizontal velocity components (not shown here) of the first mode have a node between level 6 and level 7, while those of the second baroclinic mode have maximum amplitudes at level 1, level 6, and level 8. Hence the second mode is dominant in the horizontal motion at level 6, which is seen in Fig. 4-2-14(e). Rossby waves due to reflections at the eastern boundary are not clearly seen, especially in the temperature changes.

Figs. 4-2-15 and 4-2-16 show anomaly variations in case 120 and case 130. In the anomalously forced region, the response is qualitatively similar within the three. To the east of the forced region, temperature anomalies are produced as far as the eastern boundary, whereas to the west, significant anomalies are confined to the vicinity of the forced region. Velocity anomalies, in contrast to temperature anomalies, propagate westward as well as eastward, although westward propagating signals are generally weak. Thus, the equatorial region west of the forced region is less affected compared with the region to the east. The reason is related to the presence of the eastward undercurrent (Philander, 1981). Fig. 4-2-17 shows the temperature anomalies of case 130. The pattern in the forced region on

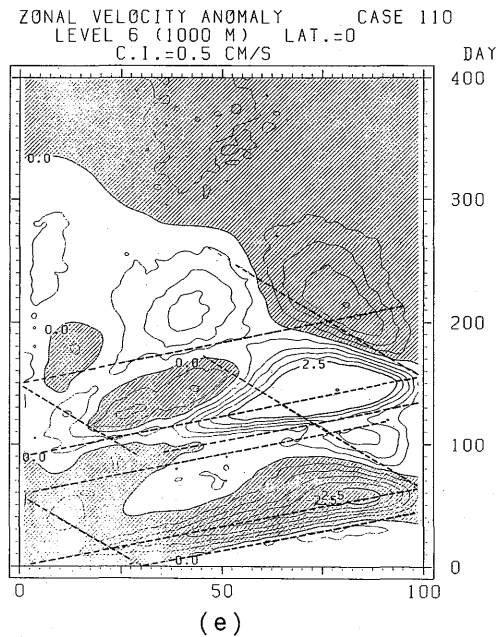


Fig. 4-2-14 Continued.

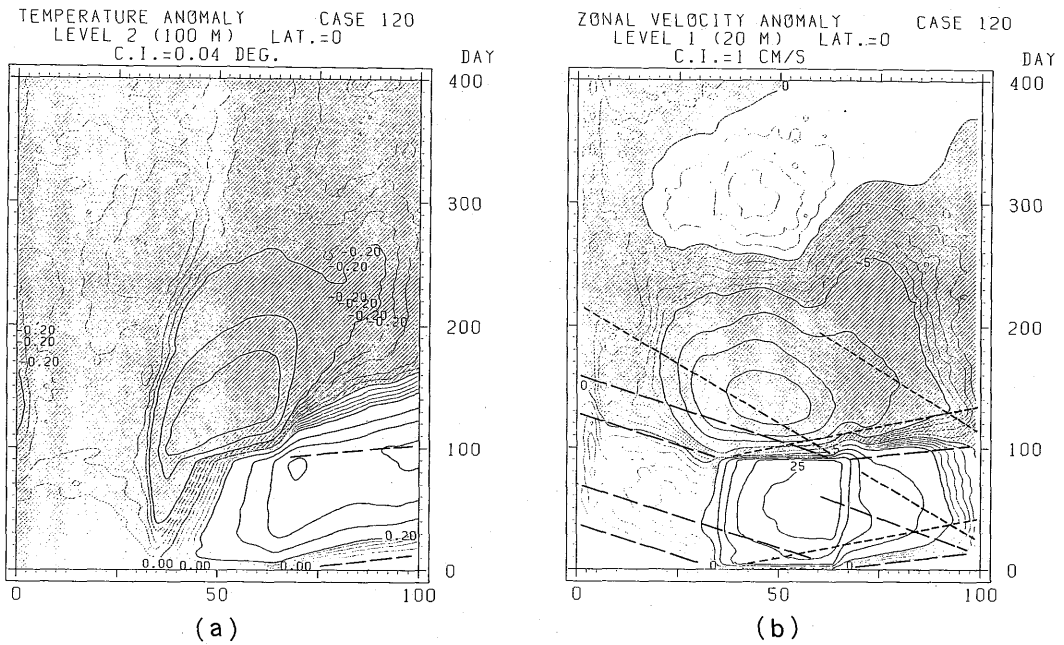


Fig. 4-2-15 Evolution of (a) the temperature anomalies at level 2 and (b) zonal velocity anomalies at level 1 along the equator in case 120.

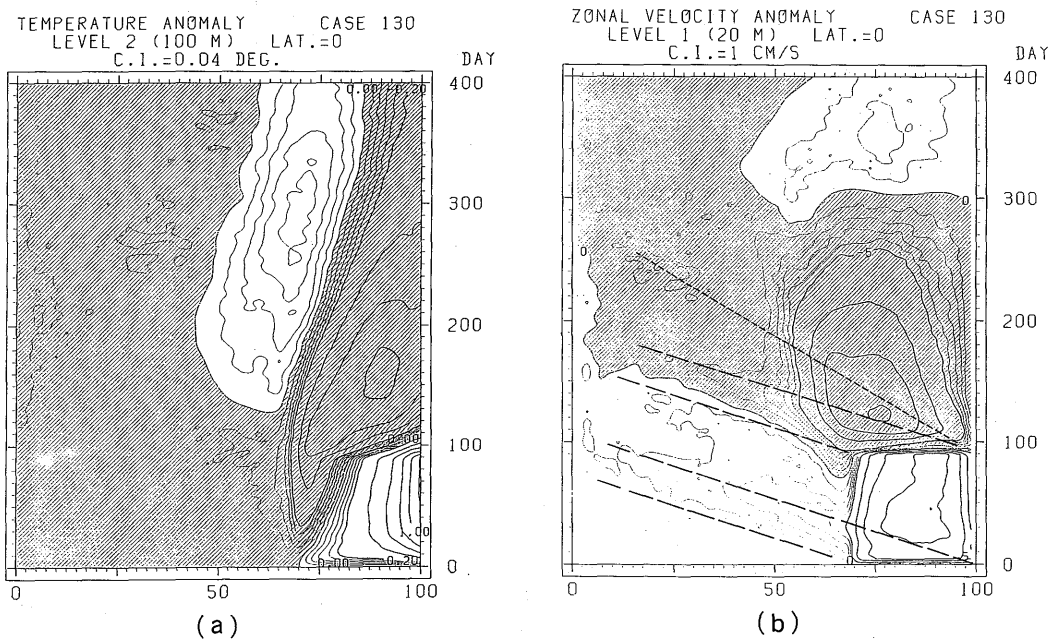


Fig. 4-2-16 As in Fig. 4-2-15 except for case 130.

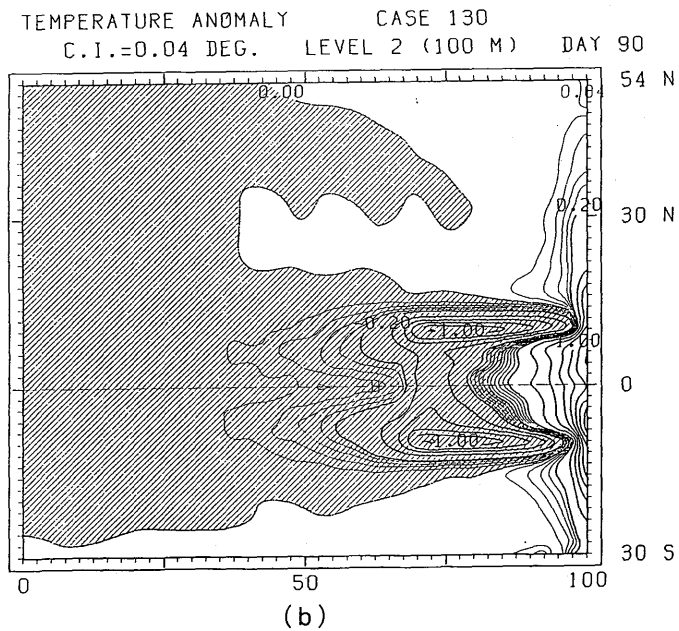
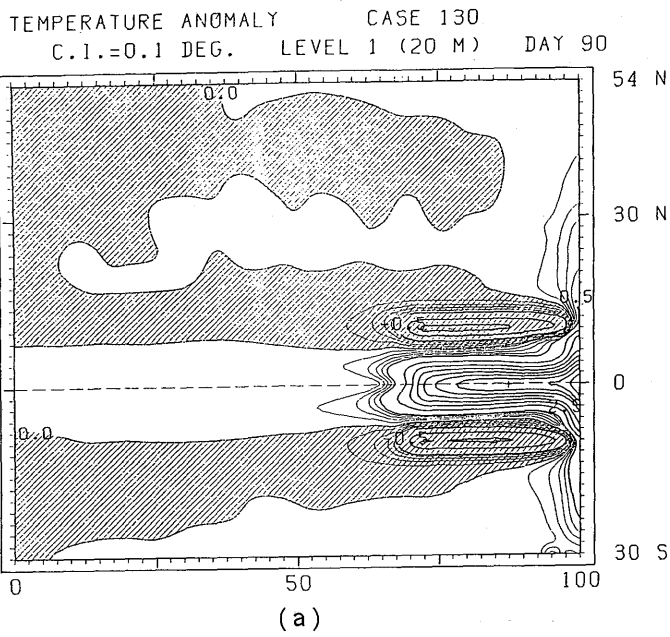


Fig. 4-2-17 As in Fig. 4-2-13 except for case 130.

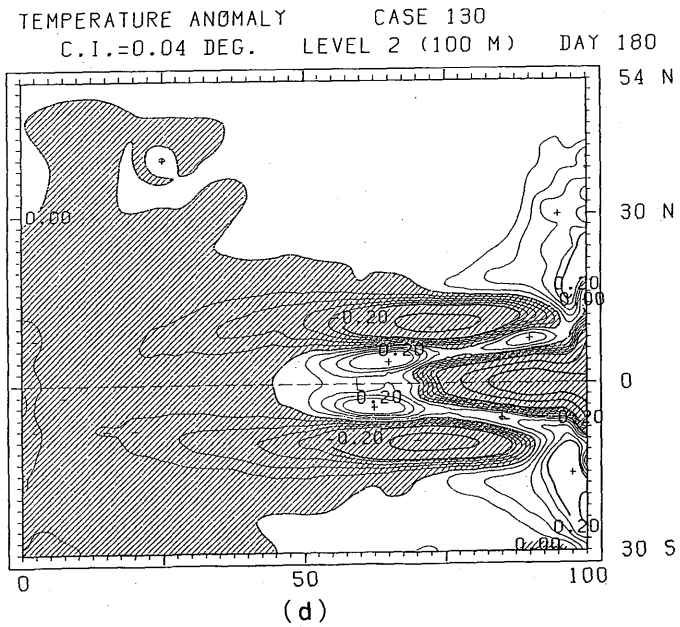
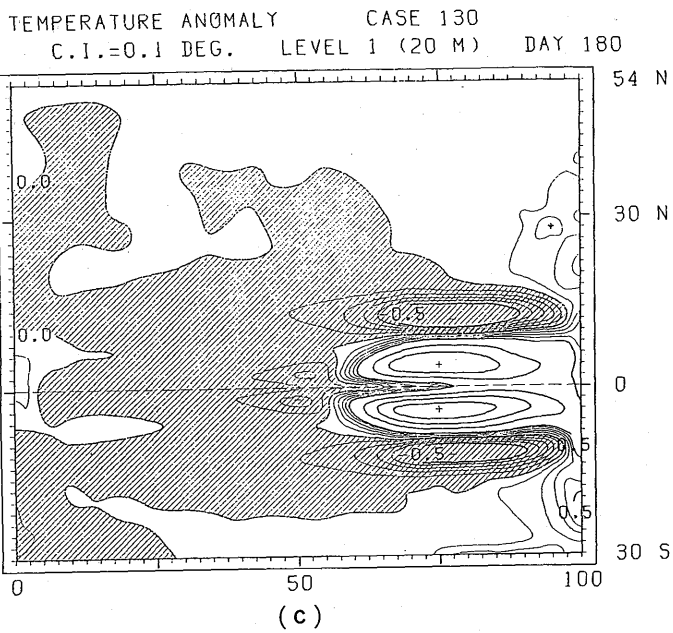


Fig. 4-2-17 Continued.

day 90 is almost the same as that of case 110 (Figs. 4-2-13 (a) and (b)) except near the eastern and western edges. The cold anomalies generated on either side of the equator propagate to the west in contrast to the temperature changes along the equator (see Fig. 4-2-17 (d)).

4.3 Response to anomalous forcing in the extra-equatorial ocean

4.3.1 Anomalous trade wind increase (cases 200 and 201)

In case 200, anomalous westward winds are imposed in the eastern two-thirds of the tropical and subtropical ocean (0° – 30° N) for 180 days (day 1—day 180) (Table 4-1-1(a), Fig. 4-1-1(c)). The maximum wind stress anomaly of 0.35 dyne/cm^2 increases the normal westward stress at 15° N by about 50%. The purpose of the experiment is to see how the thermal field evolves in response to an abrupt intensification of the trade winds.

The anomalous westward winds induce anomalous northward Ekman currents in the surface layer. The Ekman currents converge on the north side of 11° N and diverge on the south side. (Due to the meridional variation of the Coriolis parameter, the maximum Ekman currents are induced on the south side of the latitude of the maximum wind stress anomaly.) The horizontal convergence and divergence induce anomalous vertical advection of heat. Consequently, a pair of anomalous warm temperature and cold temperature develops in the forced region. The northward advection of normal temperature field by the anomalous Ekman currents (up to about 2 cm/sec) amplifies both the warm and the cold anomalies at level 1 because warm water is located along 8° N (Fig. 3-3(a)). Moreover, horizontal advection of normal temperature field by the anomalous geostrophic currents associated with the anomalous temperatures plays a significant role in the anomaly development at upper levels, especially at level 1.

Fig. 4-3-1 shows the temperature anomalies of level 1 and level 3 on day 180 when the anomalous winds are instantaneously turned off. A warm anomaly is generated to the north of 12° N and a cold anomaly to the south. The anomaly distribution is different between level 1 and level 3. The anomalies of level 1, centered at (20° N, 62.5° E) and (6° N, 70° E), are mostly confined to the forced region, while those of level 3 are displaced westward. The displacement of the cold anomaly is larger than that of the warm anomaly. Fig. 4-3-2 shows the time development of anomalies at two stations where the warm and cold anomaly centers of level 1 are located on day 180. It is evident that anomaly development in the forced region is predominant at level 1. Horizontal advection of normal temperature field is the most

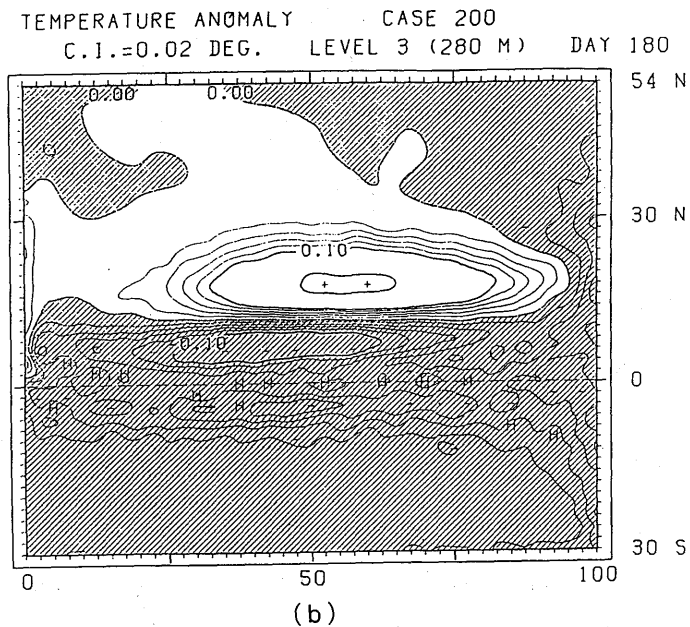
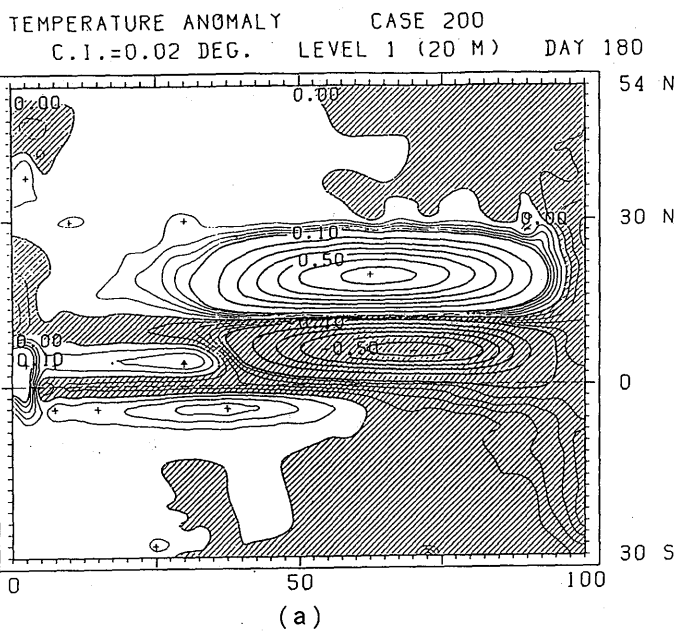


Fig. 4-3-1 Temperature anomalies on day 180 in case 200. (a) Level 1 and (b) level 3.

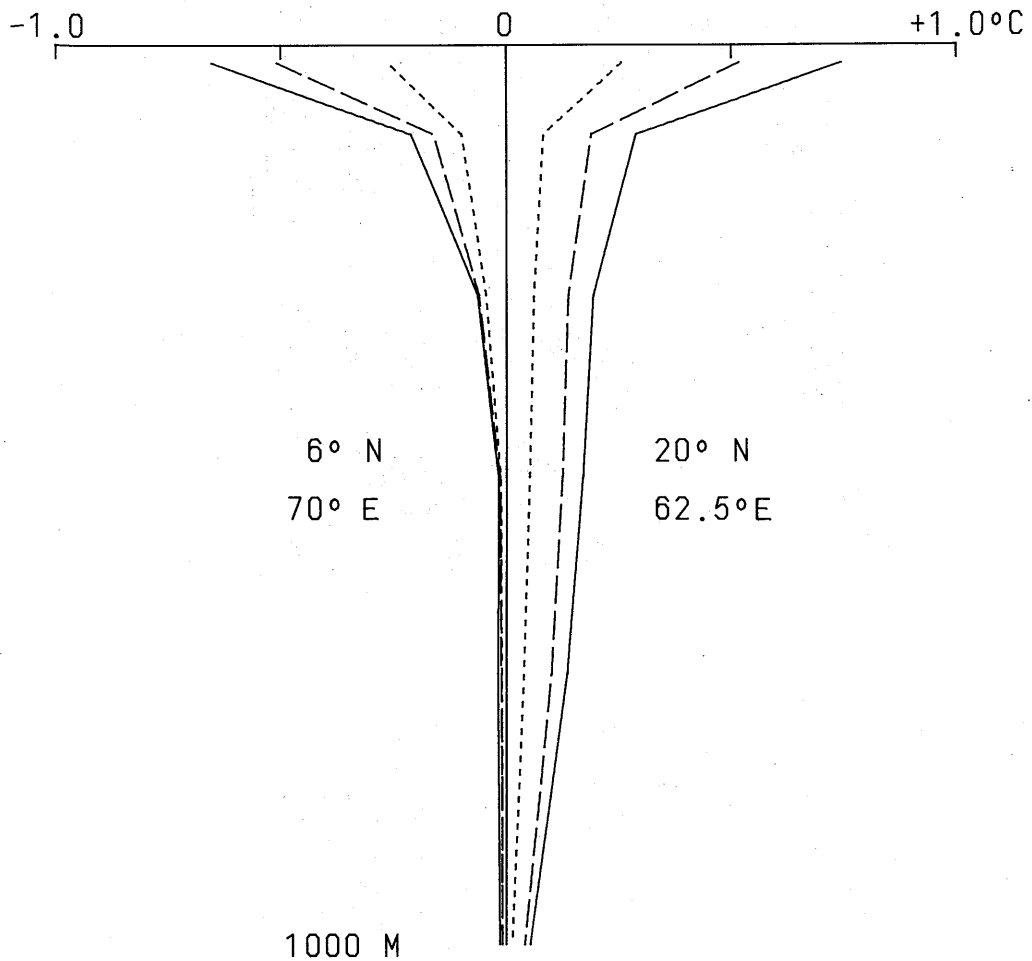


Fig. 4-3-2 Time development of the temperature anomalies at two stations, (20°N , 62.5°E) and (6°N , 70°E), in case 200. The dotted, dashed, and solid lines show the profiles on day 60, 120, and 180, respectively.

important factor in generating anomalies at level 1, which will be discussed later in connection with case 200.

The small-scale anomalies close to the western boundary in Fig. 4-3-1 are due to the meridional advection of normal temperature field by intensified western boundary currents. Although anomalous winds are imposed in the northern ocean, the anomaly distribution in the western equatorial region is symmetric about the equator. Cold anomalies are also symmetric along the eastern boundary.

Dividing the wind stress anomaly imposed in the equatorial region into a symmetric and an antisymmetric part with respect to the equator, the response in linear dynamics can be

considered as a sum of responses to the symmetric part and to the antisymmetric part. The latter response is confined to the equatorial region (McCreary, 1976). The warm anomalies on both sides of the equator of level 1 are due to the advection of warm water by the anomalous currents associated with the subsurface cold anomalies.

Fig. 4-3-3 shows zonal vertical sections through the warm and the cold anomalies in Fig. 4-3-1. There are two remarkable differences between the anomaly patterns. The first is that the warm anomaly penetrates to a greater depth than the cold anomaly. The second is that the subsurface center of the cold anomaly is displaced further westward than that of the warm anomaly. The western edge of the cold anomaly has already reached the western boundary at the subsurface (see Fig. 4-3-7 (b)). These differences are also obvious in Figs. 4-3-1 and 4-3-2. The latter difference can be attributed to the different phase speeds of Rossby waves. At 18°N , the fastest baroclinic Rossby wave propagates only 18° in longitude for 180 days, while at 6°N even the non-dispersive Rossby wave of the third baroclinic mode can propagate about 25° in longitude (Table 4-1-2).

Figs. 4-3-4 and 4-3-5 show the anomalies on day 360 and day 720, and Figs. 4-3-6 and 4-3-7 show the evolution of the temperature anomalies along 18°N and 6°N , respectively. The warm anomaly north of 12°N of level 1 expands to the west and drifts northward as a whole between day 180 and day 360. Then the anomaly is split into two parts as shown in Fig. 4-3-5(a). One of them moves east-northeastward, and the other moves westward. The propagation speed about 3 cm/sec of the eastern anomaly center is comparable to the normal current speed (Fig. 3-3(d)). Once the western anomaly arrives in the western boundary region, it moves northward along the boundary. The warm anomaly of level 3 drifts westward as a whole, then it extends northward along the western boundary.

Fig. 4-3-6 shows that the western edge of the warm anomaly of level 1 rapidly expands to the west, while the anomaly center itself slowly drifts to the west. The expansion speed is almost equal to that of the western edge of level 3, and also the propagation speed of the warm anomaly center of level 3 after day 180. This speed is approximately identical with the phase speed of the non-dispersive Rossby wave of the first baroclinic mode. The zonal component of the normal currents at 18°N , eastward at level 1 and westward at level 3, is far slower than the expansion speed.

The cold anomaly south of 12°N of level 1 is shown to have drifted northwestward as a whole between day 180 and day 720. Its center moves northward at first, then northwestward. The propagation speed is comparable to the normal current speed of 3–5 cm/sec.

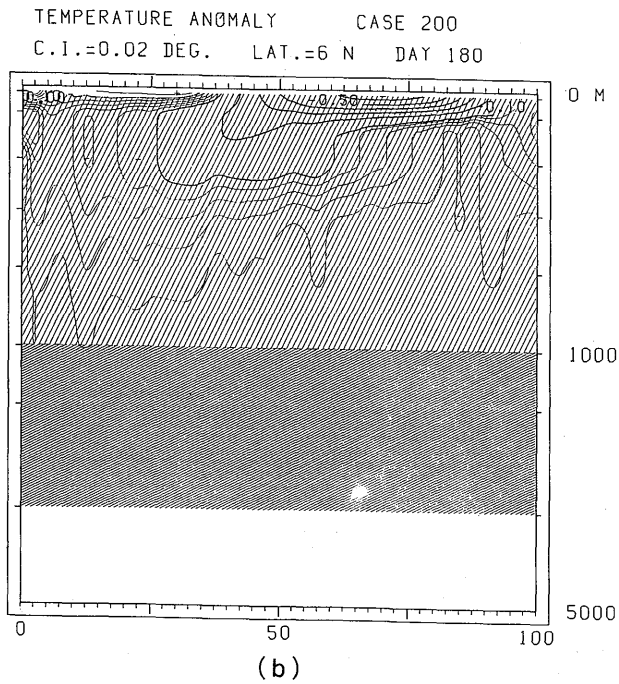
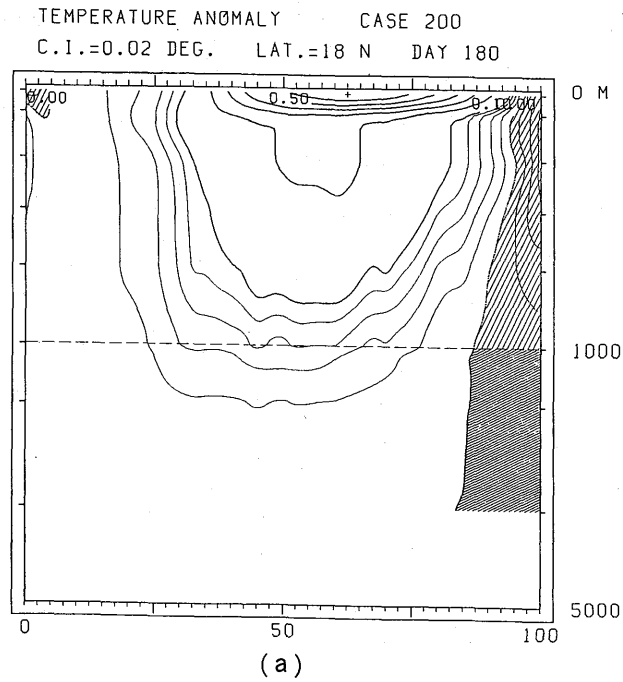
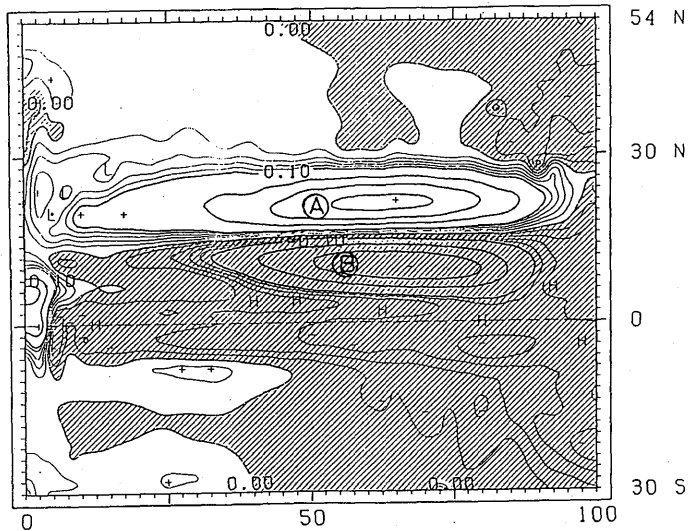


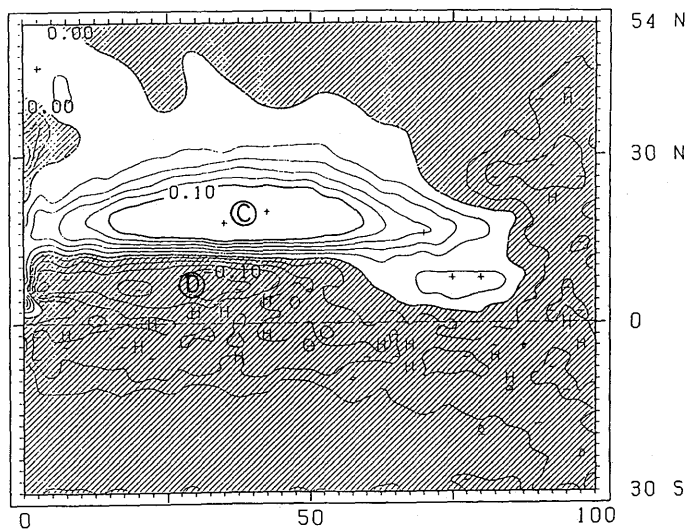
Fig. 4-3-3 Zonal cross-sections of the temperature anomalies on day 180 in case 200. (a) Along 18°N and (b) 6°N.

TEMPERATURE ANOMALY CASE 200
C.I.=0.02 DEG. LEVEL 1 (20 M) DAY 360



(a)

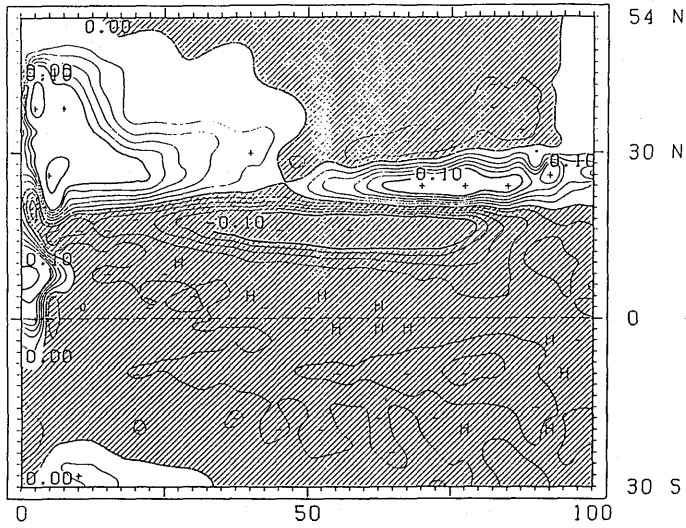
TEMPERATURE ANOMALY CASE 200
C.I.=0.02 DEG. LEVEL 3 (280 M) DAY 360



(b)

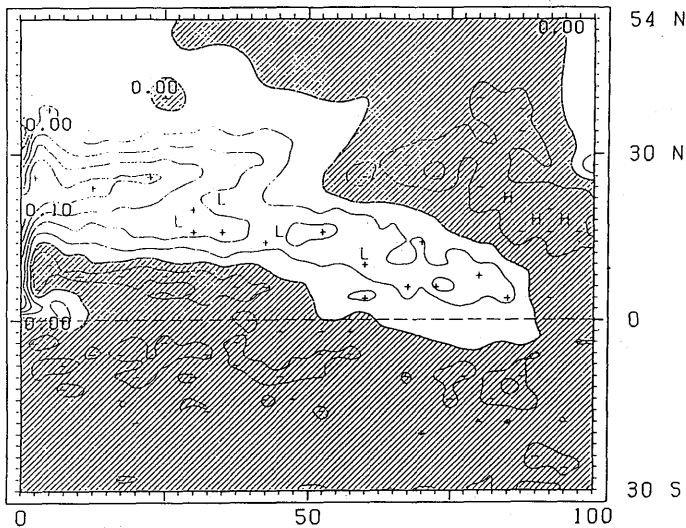
Fig. 4-3-4 As in Fig. 4-3-1 except for day 360.

TEMPERATURE ANOMALY CASE 200
C.I.=0.02 DEG. LEVEL 1 (20 M) DAY 720



(a)

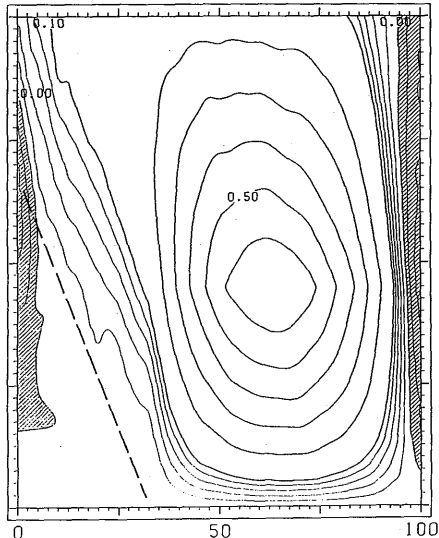
TEMPERATURE ANOMALY CASE 200
C.I.=0.02 DEG. LEVEL 3 (280 M) DAY 720



(b)

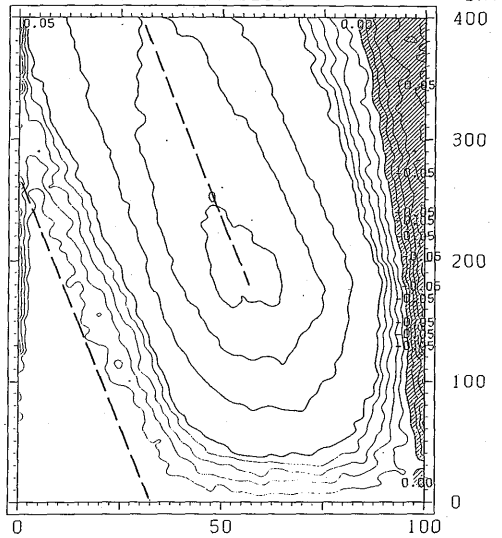
Fig. 4-3-5 As in Fig. 4-3-1 except for day 720.

TEMPERATURE ANOMALY CASE 200
LEVEL 1 (20 M) LAT.=18 N
C.I.=0.02 DEG.



(a)

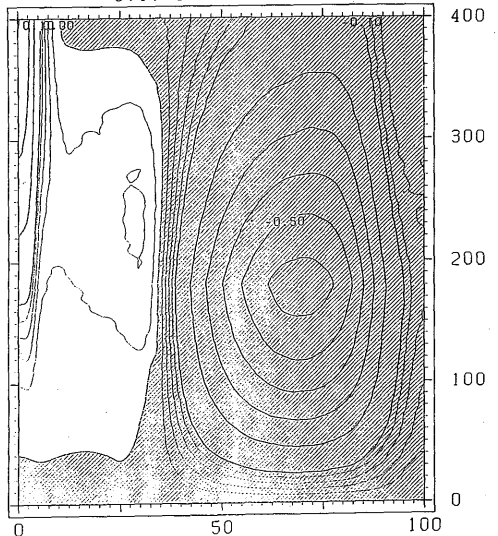
TEMPERATURE ANOMALY CASE 200
LEVEL 3 (280 M) LAT.=18 N
C.I.=0.01 DEG.



(b)

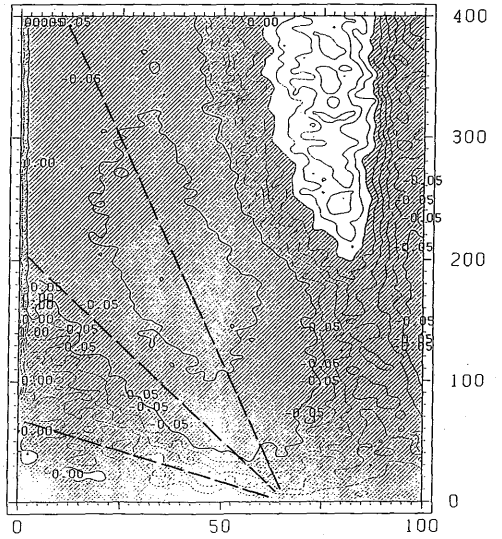
Fig. 4-3-6 Temperature anomaly variations along 18°N in case 200. (a) Level 1 and (b) level 3. The dashed lines correspond to the phase speed of the non-dispersive Rossby wave of the first baroclinic mode.

TEMPERATURE ANOMALY CASE 200
LEVEL 1 (20 M) LAT.=6 N
C.I.=0.02 DEG.



(a)

TEMPERATURE ANOMALY CASE 200
LEVEL 3 (280 M) LAT.=6 N
C.I.=0.01 DEG.



(b)

Fig. 4-3-7 As in Fig. 4-3-6 except for 6°N. The dashed lines correspond to the phase speeds of the non-dispersive Rossby waves for the first three baroclinic modes.

At level 3, on the other hand, the cold anomaly drifts westward, and anomalously warm temperatures newly develop in the region where the cold anomaly was initially generated.

Fig. 4-3-7 shows that the cold anomaly of level 1 is nearly stationary in the east-west direction, while that of level 3 drifts westward. The reason why the western edge of the cold anomaly at level 1 does not expand to the west is that the anomalous horizontal advection of the normal temperature field generates warm anomalies (see Fig. 4-3-1(b)). The anomaly center of level 3 propagates at the phase speed of the non-dispersive Rossby wave of the third baroclinic mode.

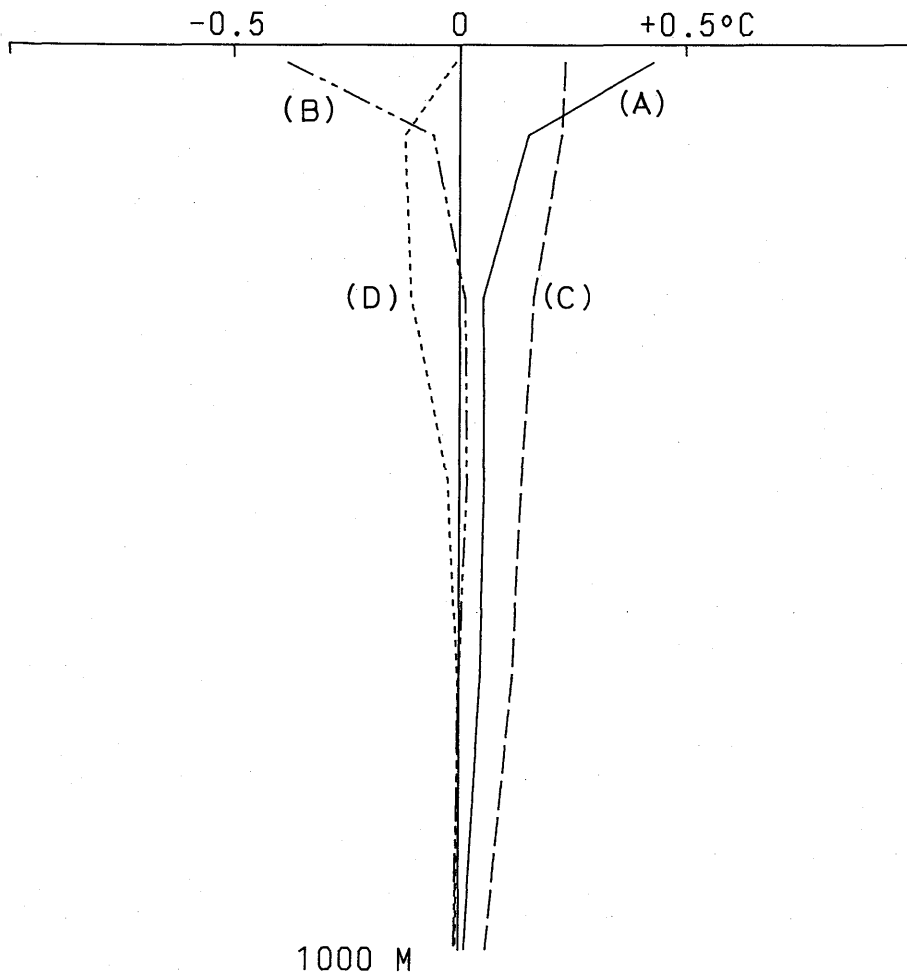


Fig. 4-3-8 Vertical structure of the temperature anomalies on day 360 in case 200. Full line: anomaly (A) at (22°N, 62.5°E), two dots and dashed line: anomaly (B) at (10°N, 65°E), dashed line: anomaly (C) at (20°N, 37.5°E) and dotted line: anomaly (D) at (8°N, 32.5°E).

Fig. 4-3-8 shows the vertical structure of anomalies (A), (B), (C), and (D) marked in Fig. 4-3-4. The eastern two anomalies, warm anomaly (A) and cold anomaly (B) of level 1, have a maximum value at the surface. On the other hand, the western two anomalies, warm anomaly (C) and cold anomaly (D) of level 3, have significant signals at the subsurface. The subsurface signals are comparable with or larger than those at the surface. Another point to be noted is that the warm anomalies (A) and (C) penetrate deeper than the cold anomalies (B) and (D). Anomaly (D) has a higher mode structure than the temperature changes associated with the first baroclinic mode (see Fig. 4-1-2(b)).

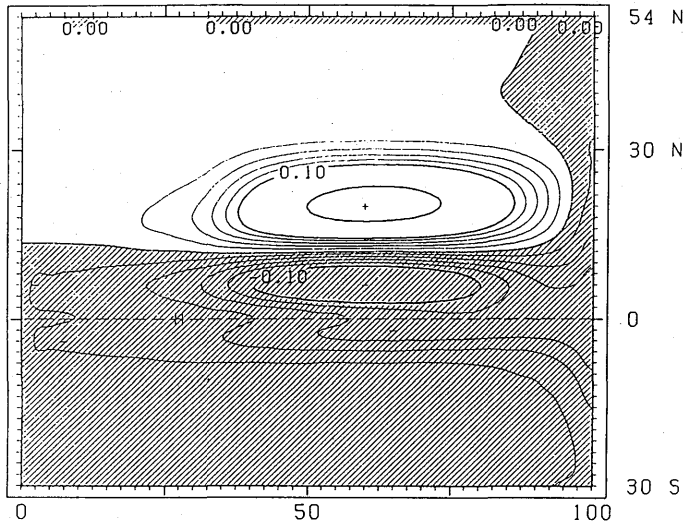
The same anomalous winds as those for case 200 are used for *case 201, the normal state of which is horizontally uniform and motionless*. The initial stratification is that of case 200 averaged over the region from the equator to 30°N and from 0° to 100°E.

Fig. 4-3-9 shows the results on day 360. Between Figs. 4-3-4 and 4-3-9, the following two differences are remarkable. First, the anomalies at level 1 are much smaller in magnitude in case 201 than in case 200. In case 201, anomalies are essentially produced by anomalous vertical motion (Ekman pumping) (term (E) in Eq. (4-1)). In case 200, on the other hand, they are produced by anomalous Ekman currents (The difference in the magnitudes at level 3 is chiefly due to different vertical structures of normal temperature field.) The second is that the westward expansion of the warm anomaly of level 1 is slower in case 201 than in case 200, and the westward displacement of the warm anomaly center of level 3 is also slower. Anomalous horizontal advection of normal temperature field, in this case mainly by anomalous geostrophic currents associated with subsurface anomalies, can explain a large part of this difference. Differences arising from the effect of advection by normal currents (terms (C) and (D)) become clear after day 360. Neither a northward displacement of surface anomalies nor a splitting of a surface anomaly center as in Fig. 4-3-5(a) are seen in case 201.

4.3.2 Variation 1 (case 210)

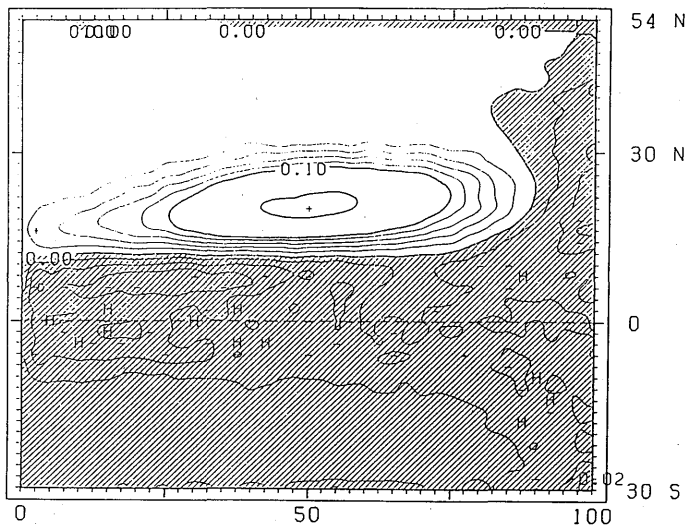
In this experiment, anomalous westward winds are imposed in a narrower region and for a shorter period than in case 200 (Table 4-1-1(a), Fig. 4-1-1(d)). A warm anomaly centered around 18–20°N is formed to the north of 14°N, and a cold anomaly is formed around 10°N. Their evolution after day 90 is essentially the same as that in case 200. In the equatorial region no significant anomalies appear except at the western boundary, though small amplitude signals are discerned to propagate eastward along the equator.

TEMPERATURE ANOMALY CASE 201
C.I.=0.02 DEG. LEVEL 1 (20 M) DAY 360



(a)

TEMPERATURE ANOMALY CASE 201
C.I.=0.02 DEG. LEVEL 3 (280 M) DAY 360



(b)

Fig. 4-3-9 As in Fig. 4-3-1 except for day 360 in case 201.

4.3.3. A warm anomaly (case 250)

This experiment is intended to examine the evolution of existing anomalies. A warm anomaly is introduced in the central tropics at the initial time (Table 4-1-1(b), Fig. 4-1-1(e)). No anomalous wind forcing is introduced. The initial anomaly is uniform from the surface to a depth of 380 m and none below 380 m. The initial field is not in geostrophic balance because no anomalous currents are imposed at the initial time. The current in the model rapidly adjusts to the specified density structure ($1/f \sim 0.3$ days at 14°N). Only the low frequency transient behavior of the model ocean after the initial adjustment is concerned in this experiment.

Fig. 4-3-10 shows the anomalies of level 1 and level 4 on day 120. A pair of cold and warm anomaly under the imposed warm anomaly as shown in Fig. 4-3-10(b), is formed in the lower five levels within 10 days. The cold and the warm anomalies continue to intensify for about half a year and a few months, respectively. The warm anomaly imposed in the upper three levels rapidly elongates westward, although the movement of its center is very slow.

Fig. 4-3-11 shows a zonal vertical section through the anomaly center. The warm anomaly center of level 5 which is located at 25°E on day 120 moves westward at the speed of the non-dispersive Rossby wave of the first baroclinic mode. Along with the movement of this deep anomaly, the warm anomaly in the upper levels extends westward. After it arrives in the western boundary region, it extends further northward and southward along the western boundary. The northward extension, which is obvious in the upper two levels, is due to advection by the boundary currents. On the other hand, the southward extension and subsequent eastward extension along the equator occurs as a result of the propagation of Kelvin waves. The anomalies on day 300 are shown in Fig. 4-3-12.

4.4 Summary and remarks

Numerical experiments to investigate the formation and evolution of large-scale thermal anomalies in the upper ocean were presented in this chapter. The experiments were performed with prescribed anomalies in the zonal wind stress. The anomalies, constant in time, were imposed in the equatorial and in the tropical and subtropical region for 90 or 180 days. Integrations were carried out for a few years.

The results show that temperature anomalies, both surface and subsurface, are initially generated by anomalous winds through wind-induced anomalous advection of normal temper-

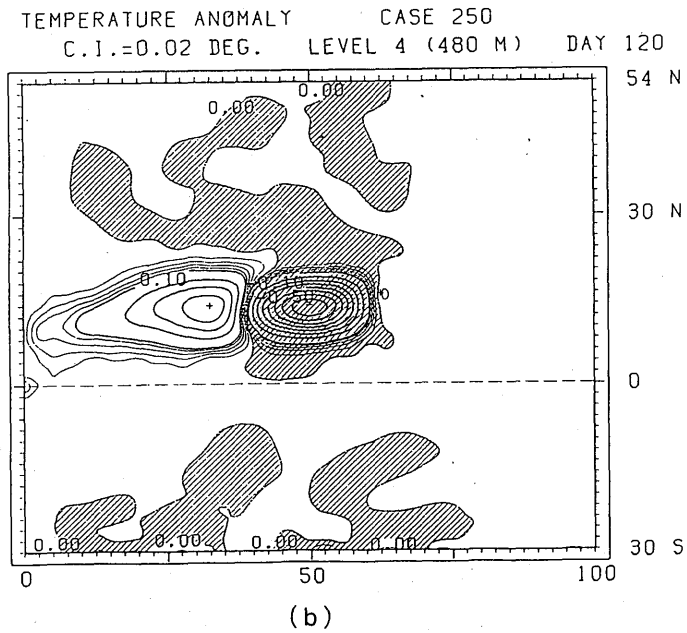
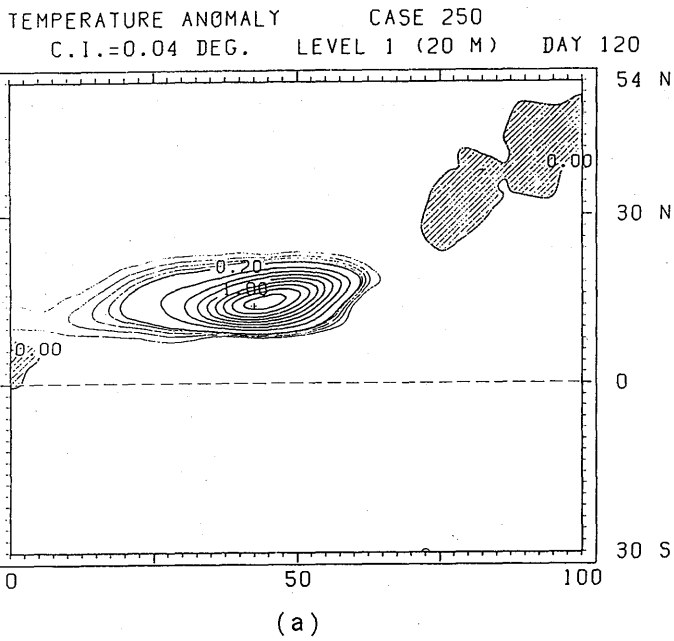


Fig. 4-3-10 Temperature anomalies on day 120 in case 250.
(a) Level 1 and (b) level 4.

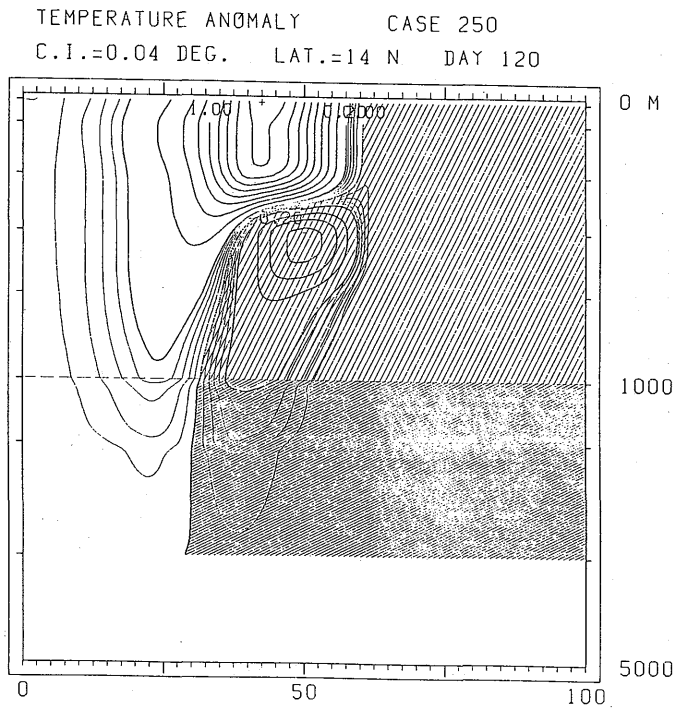


Fig. 4-3-11 A zonal cross-section of the temperature anomalies along 14°N on day 120 in case 250.

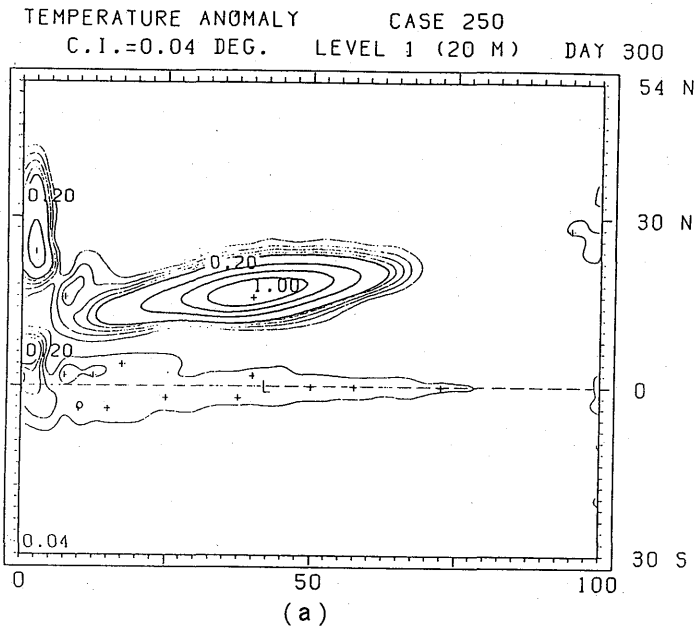


Fig. 4-3-12 As in Fig. 4-3-10 except for day 300.

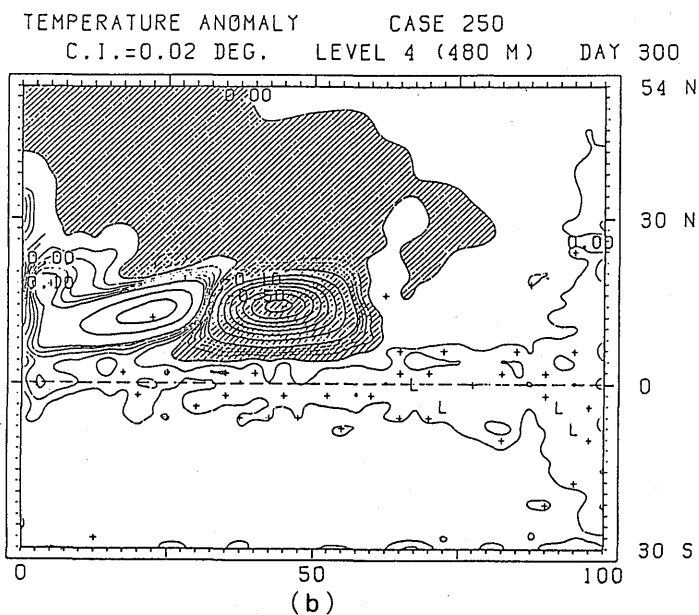


Fig. 4-3-12 Continued.

ature field. Horizontal advection (terms (A) and (B) in Eq. (4-1)) plays the most important role in the surface anomaly generation, and vertical advection (term (E)) in the subsurface anomaly generation. Once temperature anomalies are generated, all the other terms in Eq. (4-1) come into play. The horizontal advection of anomalies by normal currents (terms (C) and (D)) is one of the dominant processes in the upper ocean.

In the extra-equatorial ocean, an initially generated anomaly separates into a surface mode anomaly and a baroclinic mode anomaly. The surface mode anomaly is confined to the uppermost level, and is mainly advected by normal currents. The baroclinic mode anomaly has a significant subsurface signal, and may be accompanied with a surface signal generated due to the advection of normal temperature field by anomalous geostrophic currents associated with the subsurface anomaly. The baroclinic mode anomaly propagates westward at a speed comparable to that of a low baroclinic mode Rossby wave. However, the speed depends on the latitude of anomalously forced region and possibly on the duration and zonal extent of anomalous forcing. When the deep mode anomaly arrives in the western boundary region, a new surface mode anomaly is formed along with Kelvin mode anomalies. The Kelvin mode anomalies propagate equatorward and further eastward along the equator. The new surface mode anomaly tends to propagate or extend poleward through the effect of

advection by the western boundary currents.

In the equatorial ocean, surface mode anomalies are formed in the anomalously forced region, whereas baroclinic mode anomalies rapidly reach the eastern boundary region. Furthermore, new anomalies develop even after anomalous winds are turned off. This is one of the striking differences between responses in the equatorial ocean and the extra-equatorial ocean. The relative importance of each term in Eq. (4-1) depends not only on the latitude but also on large-scale features of the model ocean, such as current pattern and temperature gradient.

The results from this study must be verified and modified using improved models because the present model has a lot of limitations. The normal currents are far slow in comparison with observed currents. The thermocline is not always reproduced properly. The seasonal variation of the normal state is not included. Moreover, the dissipation of anomalies can not be examined with this model because of its highly diffusive nature. The attenuation of baroclinic waves is an important problem for remote forcing.

In spite of the above limitations, however, the results presented here seem to be qualitatively supported by some observational studies.

Favorite and McLain (1973) showed an example of movement of sea surface temperature anomalies in the direction of the North Pacific Current. Gill (1982) analyzed bathythermograph data from the equatorial Pacific during the period 1971–73, and described the changes in subsurface thermal structure associated with the 1972 El Niño. He showed that the changes in the central Pacific and along the eastern boundary were quite distinct. For example, subsurface temperature anomalies did not correlate well with surface temperature anomalies in the central Pacific, but they did along the eastern boundary. Gill (1983) indicated that horizontal advection of normal temperature field by anomalous zonal currents was the primary cause of the surface temperature anomalies in the central Pacific and that near the eastern boundary both anomalous horizontal advection of normal temperature field and upwelling of anomalously warm water significantly contributed to produce surface temperature anomalies. He noted further that once the surface temperature anomalies were created, advection of anomalies by normal currents became significant in spreading the anomalies over a wide range of latitudes.

White et al. (1985) investigated variability in both sea surface temperature and vertically averaged upper ocean (0–400 m) temperature over the Pacific from 20°S to 50°N. They observed that vertically averaged temperature anomalies off the equator propagated

westward at baroclinic Rossby wave speeds, and those at the equator propagated eastward at Kelvin wave speeds. They further observed that sea surface temperature anomalies propagated in the direction of normal surface currents.

Input in the present experiments were anomalies in the zonal wind stress, which are only a part of the anomalous atmospheric forcing responsible for the generation of temperature anomalies. The importance of anomalous surface heating and anomalous vertical mixing due to surface-generated turbulence was pointed out by Haney (1980), who attempted to simulate numerically observed behavior of large-scale thermal anomalies in the central North Pacific.

Elsberry and Garwood (1978) examined sea surface temperature changes at Ocean Weather Station Papa, and demonstrated that synoptic-scale atmospheric disturbances are important for the development of upper-ocean temperature anomalies. The anomalies produced by different forcing would have different vertical structure, so that their evolution is considered to be different. Further experiments using more realistic atmospheric forcing are needed. In the present study, changes in a model ocean induced by local atmospheric forcing were traced down for a few years, but ocean-atmosphere interactions were not included. In nature, anomalies in the sea surface temperature have great impact on the large-scale atmospheric circulation. Subsequent changes in the atmospheric circulation, in turn, tend to modify or newly generate sea surface temperature anomalies. This effect can be studied only by ocean-atmosphere coupled models.

References

- Bryan, K., 1969a: A numerical method for the study of the circulation of the world ocean. *J. Comput. Phys.*, **4**, 347-376.
- Bryan, K., 1969b: Climate and the ocean circulation: III. The ocean model. *Mon. Wea. Rev.*, **97**, 806-827.
- Bryan, K., and M.D. Cox, 1968: A nonlinear model of an ocean driven by wind and differential heating: Part 1. Description of the three-dimensional velocity and density fields. *J. Atmos. Sci.*, **25**, 945-967.
- Dorman, C. E. and R. H. Bourke, 1979: Precipitation over the Pacific Ocean, 30°S to 60°N. *Mon. Wea. Rev.*, **107**, 896-910.
- Elsberry, R. L., and R. W. Garwood, Jr., 1978: Sea surface temperature anomaly generation in relation to atmospheric storms. *Bull. Amer. Meteor. Soc.*, **59**, 786-789.
- Favorite, F., and D. R. McLain, 1973: Coherence in transpacific movements of positive and negative anomalies of sea surface temperature, 1953-60. *Nature*, **244**, 139-143.
- Gill, A. E., 1982: Changes in thermal structure of the equatorial Pacific during the 1972 El Niño as revealed by bathythermograph observations. *J. Phys. Oceanog.*, **12**, 1373-1387.
- Gill, A. E., 1983: An estimation of sea-level and surface-current anomalies during the 1972 El Niño and consequent thermal effects. *J. Phys. Oceanog.*, **13**, 586-606.
- Han, Y.-J., 1975: Numerical simulation of mesoscale ocean eddies. Ph. D. Thesis, Dept. Meteorol., University of California, 153pp.
- Haney, R. L., 1971: Surface thermal boundary condition for ocean circulation models. *J. Phys. Oceanog.*, **1**, 241-248.
- Haney, R. L., 1974: A numerical study of the response of an idealized ocean to large-scale surface heat and momentum flux. *J. Phys. Oceanog.*, **4**, 145-167.
- Haney, R. L., 1980: A numerical case study of the development of large-scale thermal anomalies in the central North Pacific Ocean. *J. Phys. Oceanog.*, **10**, 541-556.
- Kutsuwada, K. and K. Sakurai, 1982: Climatological maps of wind stress field over the North Pacific Ocean. *Oceanog. Mag.*, **32**, 25-46.
- Leetmaa, A., J. P. McCreary, Jr., and D. W. Moore, 1981: Equatorial currents: observations and theory. In *Evolution of Physical Oceanography*, B. A. Warren and C. Wunsch,

- eds., The MIT Press, 184-196.
- McCreary, J., 1976: Eastern tropical ocean response to changing wind systems: with application to El Niño. *J. Phys. Oceanog.*, **6**, 632-645.
- Moore, D. W., and S. G. H. Philander, 1977: Modeling of the tropical oceanic circulation. In *The Sea*, Vol. 6, Wiley-Interscience, New York, 319-361.
- Philander, S. G. H., 1981: The response of equatorial ocean to a relaxation of the trade winds. *J. Phys. Oceanog.*, **11**, 176-189.
- Rasmusson, E. M., and T. H. Carpenter, 1982: Variations in tropical sea surface temperature and surface wind fields associated with the Southern Oscillation/El Niño. *Mon. Wea. Rev.*, **110**, 354-384.
- Semtner, A. J., 1974: An oceanic general circulation model with bottom topography. *Numerical Simulation of Weather and Climate*, Tech. Rept. No. 9, Dept. Meteorol., University of California, 99pp.
- Semtner, A. J., and Y. Mintz, 1977: Numerical simulation of the Gulf Stream and mid-ocean eddies. *J. Phys. Oceanog.*, **7**, 208-230.
- Takano, K., 1974: A general circulation model for the World Ocean. UCLA Dept. of Meteorology Tech. Rep. No. 8.
- Takano, K., 1981: A note on the haline, thermohaline and thermohaline-wind-driven ocean circulation. *La mer*, **19**, 185-203.
- Takeuchi, K., 1984: Numerical study of the Subtropical Front and the Subtropical Counter-current. *J. Oceanog. Soc. Japan.*, **40**, 371-381.
- Weare, B. C., P. T. Strub and M. D. Samuel, 1981: Annual mean surface heat fluxes in the tropical Pacific Ocean. *J. Phys. Oceanog.*, **11**, 705-717.
- Williams, G. P., 1969: Numerical integration of the three-dimensional Navier-Stokes equations for incompressible flow. *J. Fluid Mech.*, **37**, 727-750.
- White, W. B., G. A. Meyers, J. R. Donguy and S. E. Pazan, 1985: Short-term climatic variability in the thermal structure of the Pacific Ocean during 1979-82. *J. Phys. Oceanog.*, **15**, 917-935.
- Wyrtki, K., 1965: The average annual heat balance of the North Pacific Ocean and its relation to ocean circulation. *J. Geoph. Res.*, **70**, 4547-4559.
- Wyrtki, K., and G. Meyers, 1976: The trade wind field over the Pacific Ocean. *J. Appl. Meteor.*, **15**, 698-704.

気象研究所技術報告一覧表

- 第1号 バックグラウンド大気汚染の測定法の開発 (地球規模大気汚染特別研究班, 1978)
Development of Monitoring Techniques for Global Background Air Pollution (MRI Special Research Group on Global Atmospheric Pollution, 1978)
- 第2号 主要活火山の地殻変動並びに地熱状態の調査研究 (地震火山研究部, 1979)
Investigation of Ground Movement and Geothermal State of Main Active Volcanoes in Japan (Seismology and Volcanology Research Division, 1979)
- 第3号 筑波研究学園都市に新設された気象観測用鉄塔施設 (花房龍男・藤谷徳之助・伴野登・魚津 博, 1979)
On the Meteorological Tower and Its Observational System at Tsukuba Science City (T. Hanafusa, T. Fujitani, N. Banno and H. Uozu, 1979)
- 第4号 海底地震常時観測システムの開発 (地震火山研究部, 1980)
Permanent Ocean-Bottom Seismograph Observation System (Seismology and Volcanology Research Division, 1980)
- 第5号 本州南方海域水温図—400 m (又は 500 m) 深と 1000 m 深— (1934—1943 年及び 1954—1980 年) (海洋研究部, 1981)
Horizontal Distribution of Temperature in 400m (or 500m) and 1000m Depth in Sea South of Honshu, Japan and Western-North Pacific Ocean from 1934 to 1943 and from 1954 to 1980 (Oceanographical Research Division, 1981)
- 第6号 成層圏オゾンの破壊につながる大気成分および紫外日射の観測 (高層物理研究部, 1982)
Observations of the Atmospheric Constituents Related to the Stratospheric Ozone Depletion and the Ultraviolet Radiation (Upper Atmosphere Physics Research Division, 1982)
- 第7号 83 型強震計の開発 (地震火山研究部, 1983)
Strong-Motion Seismograph Model 83 for the Japan Meteorological Agency Network (Seismology and Volcanology Research Division, 1983)
- 第8号 大気中における雪片の融解現象に関する研究 (物理気象研究部, 1984)
The Study of Melting of Snowflakes in the Atmosphere (Physical Meteorology Research Division, 1984)
- 第9号 御前崎南方沖における海底水圧観測 (地震火山研究部・海洋研究部, 1984)

- Bottom Pressure Observation South off Omaezaki, Central Honshu (Seismology and Volcnology Research Division and Oceanographical Research Division, 1984)
- 第10号 日本付近の低気圧の統計 (予報研究部, 1984)
Statistics on Cyclones Around Japan (Forecast Research Division, 1984)
- 第11号 局地風と大気汚染物質の輸送に関する研究 (応用気象研究部, 1984)
Observations and Numerical Experiments on Local Circulation and Medium-Range Transport of Air Pollutions (Applied Meteorology Research Division, 1984)
- 第12号 火山活動監視手法に関する研究 (地震火山研究部, 1984)
Investigation on the Techniques for Volcanic Activity Surveillance (Seismology and Volcanology Research Division, 1984)
- 第13号 気象研究所大気大循環モデル-I (MRI・GCM-I) (予報研究部, 1984)
A Description of the MRI Atmospheric General Circulation Model (The MRI・GCM-I) (Forecast Research Division, 1984)
- 第14号 台風の構造の変化と移動に関する研究—台風 7916 の一生— (台風研究部, 1985)
A Study on the Changes of the Three-Dimensional Structure and the Movement Speed of the Typhoon Through Its Life Time (Typhoon Research Division, 1985)
- 第15号 波浪推算モデル MRI と MRI-II の相互比較研究—計算結果図集— (海洋研究部, 1985)
An Intercomparison Study Between the Wave Models MRI and MRI-II—A Compilation of Results— (Oceanographical Research Division, 1985)
- 第16号 地震予知に関する実験的及び理論的研究 (地震火山研究部, 1985)
Study on Earthquake Prediction by Geophysical Method (Seismology and Volcanology Research Division, 1985)
- 第17号 北半球地上月平均気温偏差図 (予報研究部, 1986)
Maps of Monthly Mean Surface Temperature Anomalies over the Northern Hemisphere for 1891—1981 (Forecast Research Division, 1986)
- 第18号 中層大気の研究 (高層物理研究部・気象衛星研究部・予報研究部・地磁気観測所, 1986)
Studies of the Middle Atmosphere (Upper Atmosphere Physics Research Division, Meteorological Satellite Research Division, Forecast Research Division, MRI. The Magnetic Observatory, 1986)
- 第19号 ドップラーレーダによる気象・海象の研究 (気象衛星研究部・予報研究部・応用気象研究部・海洋研究部, 1986)
Studies on Meteorological and Sea Surface Phenomena by Doppler Radar (Meteor-

ological Satellite Research Division, Typhoon Research Division, Forecast Research Division, Applied Meteorology Research Division, Oceanographical Research Division, 1986)

第20号 気象研究所対流圏大気大循環モデル (MRI・GCM-I) による12年間の積分 (予報研究部, 1986)

Mean Statistics of the Tropospheric MRI・GCM-I based on 12-year Integration (Forecast Research Division, 1986)

第21号 宇宙線中間子強度1983—1986 (高層物理研究部, 1987)

Multi-Directional Cosmic Ray Meson Intensity 1983—1986 (Upper Atmosphere Physics Research Division, 1987)

第22号 静止気象衛星「ひまわり」画像の噴火噴煙データにもとづく噴火活動の解析に関する研究 (地震火山研究部, 1987)

Study on Analyses of Volcanic Eruptions based on Eruption Cloud Image Data Obtained by the Geostationary Meteorological Satellite (GMS) (Seismology and Volcanology Research Division, 1987)

第23号 オホーツク海海洋気候図 (篠原吉雄・四竈信行, 1988)

Marine Climatological Atlas of the Sea of Okhotsk Y. Shinohara and N. Shikama, 1988)

気象研究所

1946年(昭和21年)設立

所長：理博 岡村 存

予報研究部	部長：	久保田	効
気候研究部	部長：	桐山	一陽
台風研究部	部長：	蔵重	清
物理気象研究部	部長：	旭	満
応用気象研究部	部長：	眞島	恒裕
気象衛星・観測 システム研究部	部長：	鯉沼	正一
地震火山研究部	部長：理博	勝又	護
海洋研究部	部長：	佐野	昭
地球化学研究部	部長：理博	杉村	行勇

気象研究所技術報告

編集委員長：勝 又 護

編集委員：藤部文昭 木田秀次 高谷美正
忠鉢 繁 佐藤純次 内野 修
古屋逸夫 遠藤昌宏 井上久幸
事務局：松下 眞 中山和之

気象研究所技術報告は、気象学、海洋学、地震学、その他関連の地球科学の分野において、気象研究所職員が得た研究成果に関し、技術報告、資料報告及び総合報告を掲載する。

気象研究所技術報告は、1978年(昭和53年)以降、必要の都度刊行される。

平成元年3月31日発行 ISSN 0386-4049

編集兼発行所 気象研究所

茨城県つくば市長峰1-1

印刷所 株式会社 明文社

東京都中央区日本橋蛸殻町1-24-8